Future changes in climate, ocean circulation, ecosystems, and biogeochemical cycling simulated for a business-as-usual CO_2 emission scenario until year 4000 AD

Andreas Schmittner,[1] Andreas Oschlies,[2] H. Damon Matthews,[3] and Eric D. Galbraith[4]

Received 5 February 2007; revised 22 June 2007; accepted 6 September 2007; published 14 February 2008.

[1] A new model of global climate, ocean circulation, ecosystems, and biogeochemical cycling, including a fully coupled carbon cycle, is presented and evaluated. The model is consistent with multiple observational data sets from the past 50 years as well as with the observed warming of global surface air and sea temperatures during the last 150 years. It is applied to a simulation of the coming two millennia following a business-as-usual scenario of anthropogenic CO_2 emissions (SRES A2 until year 2100 and subsequent linear decrease to zero until year 2300, corresponding to a total release of 5100 GtC). Atmospheric CO_2 increases to a peak of more than 2000 ppmv near year 2300 (that is an airborne fraction of 72% of the emissions) followed by a gradual decline to ~1700 ppmv at year 4000 (airborne fraction of 56%). Forty-four percent of the additional atmospheric CO_2 at year 4000 is due to positive carbon cycle–climate feedbacks. Global surface air warms by ~10°C, sea ice melts back to 10% of its current area, and the circulation of the abyssal ocean collapses. Subsurface oxygen concentrations decrease, tripling the volume of suboxic water and quadrupling the global water column denitrification. We estimate 60 ppb increase in atmospheric N_2O concentrations owing to doubling of its oceanic production, leading to a weak positive feedback and contributing about 0.24°C warming at year 4000. Global ocean primary production almost doubles by year 4000. Planktonic biomass increases at high latitudes and in the subtropics whereas it decreases at midlatitudes and in the tropics. In our model, which does not account for possible direct impacts of acidification on ocean biology, production of calcium carbonate in the surface ocean doubles, further increasing surface ocean and atmospheric pCO_2. This represents a new positive feedback mechanism and leads to a strengthening of the positive interaction between climate change and the carbon cycle on a multicentennial to millennial timescale. Changes in ocean biology become important for the ocean carbon uptake after year 2600, and at year 4000 they account for 320 ppmv or 22% of the atmospheric CO_2 increase since the preindustrial era.

Citation: Schmittner, A., A. Oschlies, H. D. Matthews, and E. D. Galbraith (2008), Future changes in climate, ocean circulation, ecosystems, and biogeochemical cycling simulated for a business-as-usual CO_2 emission scenario until year 4000 AD, *Global Biogeochem. Cycles*, *22*, GB1013, doi:10.1029/2007GB002953.

1. Introduction

[2] During the last decades the global climate research community has established the growing influence of human greenhouse gas emissions on Earth's climate. This research has culminated every 6 years in the publication of the assessment reports (ARs) of the Intergovernmental Panel on Climate Change (IPCC). Each time a new AR has been published the impact of burning fossil fuel has become more evident as reflected in the following two statements from the three most recent successive reports. "The balance of evidence suggests a discernible human influence on global climate" (2nd AR [*IPCC*, 1995]). "There is new and stronger evidence that most of the warming observed over the last 50 years is attributable to human activities" (3rd AR [*IPCC*, 2001]). "Most of the observed increase in globally averaged temperatures since the mid-20th century is very likely due to the observed increase in anthropogenic greenhouse gas concentrations" (AR4, [*IPCC*, 2007]). The increasing knowledge about global warming has not yet been

[1] College of Oceanic and Atmospheric Sciences, Oregon State University, Corvallis, Oregon, USA.
[2] Leibniz Institute of Marine Sciences at the Christian-Albrechts University of Kiel (IFM-GEOMAR), Kiel, Germany.
[3] Planning and Environment, Concordia University, Montreal, Quebec, Canada.
[4] Atmospheric and Oceanic Sciences, Princeton University, Princeton, New Jersey, USA.

0886-6236/08/2007GB002953$12.00

paralleled with increasing action to prevent "dangerous anthropogenic interference with the climate system" as required by Article 2 of the United Nations Framework Convention on Climate Change. Instead anthropogenic carbon emissions have been increasing faster than ever during the last years [*Marland et al.*, 2006] (see also http://www.newscientist.com/article/dn10507-carbon-emissions-rising-faster-than-ever.html) and have been closely tracking business-as-usual scenarios rather than scenarios of CO_2 stabilization at levels below 650 ppmv. The long-term response of the global climate system to a continuation of the present emission trends, in which most readily available fossil fuel resources are burned and released to the atmosphere, is a matter of concern. Here we explore this scenario through simulations with a coupled intermediate complexity model of climate, ecosystems and biogeochemical cycles.

[3] Most projections of climate change, including the fully coupled ocean-atmosphere general circulation model simulations performed for the 3rd AR [*IPCC*, 2001] and AR4, have been limited to the 21st century, in some cases the next few centuries. This is also true for estimates of future climate–carbon cycle feedbacks [*Maier-Reimer et al.*, 1996; *Sarmiento et al.*, 1998; *Matear and Hirst*, 1999; *Cox et al.*, 2000; *Joos et al.*, 2001; *Dufresne et al.*, 2002; *Friedlingstein et al.*, 2003; *Jones et al.*, 2003; *Zeng et al.*, 2004; *Govindasamy et al.*, 2005; *Friedlingstein et al.*, 2006] and changes in ocean ecosystems [*Sarmiento et al.*, 2004]. However, it is clear that anthropogenic carbon will remain much longer in the climate system causing climate changes for many millennia to come [*Archer et al.*, 1998; *Loutre and Berger*, 2000; *Archer and Ganopolski*, 2005]. Hence here we present climate change projections for 2000 years into the future. Such multimillennial timescale simulations have previously been only possible with highly simplified models [*Archer et al.*, 1998; *Joos et al.*, 1999; *Knutti et al.*, 2003; *Lenton et al.*, 2006], but are now feasible with more detailed models because of increased computer power. The model we use here is much improved relative to those of previous studies with respect to the simulation of ocean circulation and ventilation, as well as the representation of the marine ecosystem and biogeochemical cycles. We will focus our discussion on these aspects of the model simulation. A detailed description of the terrestrial ecosystem and carbon cycle model response to global warming can be found in the work of *Matthews et al.* [2005b]. We provide the first estimate of the future climate–carbon cycle feedback on multimillennial timescales.

2. Model Description

[4] The UVic Earth System Climate Model [*Weaver et al.*, 2001] version 2.7 used here consists of a coarse resolution ($1.8 \times 3.6^\circ$, 19 vertical layers) three-dimensional general circulation model of the ocean (Modular Ocean Model 2) with state-of-the-art physical parameterizations such as diffusive mixing along and across isopycnals, eddy induced tracer advection [*Gent and McWilliams*, 1990] and a scheme for the computation of tidally induced diapycnal mixing over rough topography [*Simmons et al.*, 2004]. This scheme leads to low diapycnal mixing in the pycnocline with diffusivities in the open ocean of around 2×10^{-5} m^2 s^{-1}. The along isopycnal diffusivity is 2000 m^2 s^{-1} and the thickness diffusivity is 1000 m^2 s^{-1}. A simple one-layer atmospheric energy-moisture balance model interactively calculates heat and water fluxes to ocean, land and sea ice. Wind velocities are prescribed from the NCAR/NCEP monthly climatology to calculate the momentum transfer to the ocean and to a dynamic-thermodynamic sea ice model, surface heat and water fluxes, and the advection of water vapor in the atmosphere. In order to improve the simulation of precipitation over topography the atmospheric lapse rate is reduced to 30% in the calculation of the elevated saturation specific humidity. The terrestrial vegetation and carbon cycle component [*Meissner et al.*, 2003] is based on the Hadley Center model TRIFFID. Continental ice sheets are assumed to remain constant. The simulation of sea ice has been evaluated previously and found to be in good agreement with observations [*Bitz et al.*, 2001; *Saenko et al.*, 2002]. The annual mean sea ice area in the current model version is $24 \cdot 10^6$ km^2 ($12 \cdot 10^6$ km^2 in the Southern Hemisphere and $11 \cdot 10^6$ km^2 in the Northern Hemisphere) consistent with observations [*Cavalieri et al.*, 1997]. Radiocarbon ($\Delta^{14}C$) and chlorofluorocarbons (CFC11 and CFC12) are included to track the ocean's ventilation on decadal to millennial timescales. The climate sensitivity expressed as the equilibrium warming for a doubling of atmospheric CO_2 is 4°C. Note that the model version we use here (which we label 2.7B, B for Biology), is different from the default version 2.7 which was used for the upcoming IPCC AR4 runs which will be published shortly and which did not contain ocean biology.

2.1. Marine Ecosystem Model

[5] The ocean ecosystem/biogeochemical model is an improved NPZD (nutrient, phytoplankton, zooplankton, detritus) ecosystem model of *Schmittner et al.* [2005a] with a parameterization of fast nutrient recycling due to microbial activity after *Schartau and Oschlies* [2003]. It includes two phytoplankton classes (nitrogen fixers and other phytoplankton), nitrate (NO_3) and phosphate (PO_4) as nutrients, as well as oxygen (O_2), dissolved inorganic carbon (DIC) and alkalinity (ALK) as tracers. A complete description of the ecosystem model is given in Appendix A, and parameter values are listed in Table A1 in Appendix A.

2.2. Marine Carbon Cycle

[6] Formulations of air-sea gas exchange and carbon chemistry follow protocols from the Ocean Carbon-Cycle Model Intercomparison Project (OCMIP) [*Orr et al.*, 1999] as described by *Ewen et al.* [2004]. Biological uptake and release occurs in fixed elemental ratios of carbon, phosphorus, nitrogen and oxygen (see Table A1 in Appendix A for values). Production of DIC and ALK is controlled by changes in inorganic nutrients and calcium carbonate ($CaCO_3$), in molar numbers according to

$$S(\mathrm{DIC}) = S(\mathrm{PO_4})R_{C:P} - S(\mathrm{CaCO_3}) \quad (1)$$

$$S(\mathrm{ALK}) = -S(\mathrm{NO_3}) \times 10^{-3} - 2S(\mathrm{CaCO_3}). \quad (2)$$

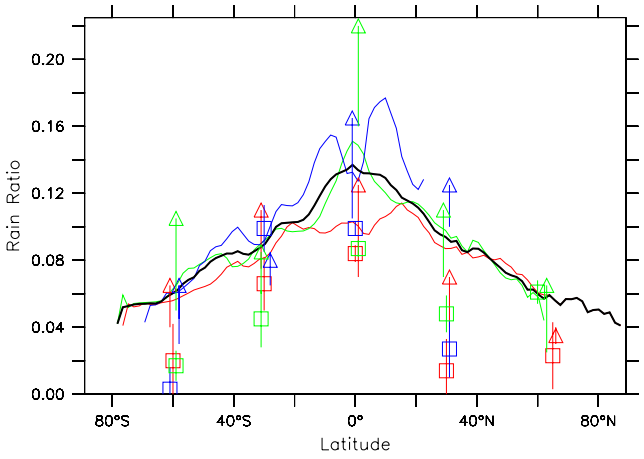

Figure 1. Ratio of calcium carbonate versus particulate organic carbon export flux (rain ratio) across 126-m depth and zonally averaged over the Atlantic (red), Pacific (green), and Indian Ocean (blue) basins in comparison with observational estimates from *Sarmiento et al.* [2002] (square symbols) and *Jin et al.* [2006] (triangles) including their reported error bars (vertical lines). Global model mean is shown as the thick solid line. Rain ratio was first calculated at each model grid point and then averaged zonally. However, first averaging the individual fluxes and then calculating the ratio leads to almost identical results.

S(X) denotes the source minus sink term for tracer X and $R_{C:P}$ is the carbon to phosphorus ratio (see Table A1 in Appendix A) The sources minus sink term of calcium carbonate $S(CaCO_3)$ = $Pr(CaCO_3)$ − $Di(CaCO_3)$ is determined by its production

$$\mathrm{Pr(CaCO_3)} = \left((1-\gamma_1)G(\mathrm{P}_O)\mathrm{Z} + \mu_{P2}\mathrm{P}_O^2 + \mu_Z\mathrm{Z}^2\right)R_{\mathrm{CaCO3/POC}}R_{C:P}, \tag{3}$$

which is parameterized as a fixed ratio ($R_{CaCO3/POC}$) of the production of nondiazotrophic detritus. In our model, none of the above processes explicitly depends on temperature. However, maximum phytoplankton growth and microbial remineralization rates are assumed to increase with temperature according to *Eppley* [1972] (see equations (A10), (A14), and (A16) in Appendix A), and as a result the production of $CaCO_3$ tends to increase with temperature as well. A similar temperature dependence is expected for other ecosystem models that parameterize calcium carbonate production as a function of primary production [e.g., *Moore et al.*, 2002]. The dissolution of calcium carbonate,

$$Di(\mathrm{CaCO_3}) = \int Pr(\mathrm{CaCO_3})dz \cdot \frac{d}{dz}\left(e^{-z/D_{\mathrm{CaCO_3}}}\right), \tag{4}$$

is computed by assuming instantaneous sinking with an e-folding depth D_{CaCO3} = 3500 m of the vertically integrated production. The strength of the calcium carbonate pump and hence the vertical alkalinity distribution is strongly determined by the parameter $R_{CaCO3/POC}$ = 0.035. This value was found to generate a globally averaged vertical ALK profile close to the observed one.

[7] The resulting ratio of organic versus carbonate export flux (rain ratio) across 126-m depth is shown in Figure 1 in comparison with recent observational estimates [*Sarmiento et al.*, 2002; *Jin et al.*, 2006]. The global mean of 0.097 in the model is consistent with the range (0.07–0.11) from different recent estimates based on observations [*Lee*, 2001; *Sarmiento et al.*, 2002] or a combination of observations and models [*Jin et al.*, 2006]. The model simulates a strong latitudinal dependence of the rain ratio with higher values of ∼0.15 at low latitudes and lower values of ∼0.05 at high latitudes. Interbasin differences are small except for the tropics where higher values are simulated in the Indian and Pacific oceans compared with the Atlantic. These patterns appear to be consistent with the observational estimates [*Sarmiento et al.*, 2002; *Jin et al.*, 2006]. In the model they are due to faster nutrient recycling in the euphotic zone at higher temperatures and hence higher $CaCO_3$ production. Export of particulate organic carbon (POC), on the other hand, does not depend much on temperature since it is more strongly controlled by the nutrient input to the euphotic zone and thus by ocean circulation. The agreement of the simulated zonally averaged patterns with observational estimates provides some independent support for our formulation of calcium carbonate production (equation (3)).

[8] Note that the model does not at present include interactions with carbonate sediments in the ocean. Calcium carbonate compensation (changes in carbonate preservation/dissolution in the sediments as a response to changes in the carbonate ion concentration of sea water) is thought to be an important feedback only on longer timescales O(5000 years) [*Archer et al.*, 1998] than considered here, although they might become significant already after ∼1700 years and thus would alter the later parts of our simulations [*Ridgwell and Hargreaves*, 2007].

3. Model Evaluation

[9] First, a model spin up of more than 10,000 years has been performed, using preindustrial boundary conditions such as insolation and an atmospheric CO_2 concentration of 280 ppmv. Subsequently the model was run with historical forcing from 1850 to 2000 using prescribed fossil fuel and land use carbon emissions from *Marland et al.* [2006] and *Houghton* [2003], estimates of shortwave volcanic, solar and anthropogenic aerosol forcing from *Crowley* [2000], changes in land use from *Ramankutty and Foley* [1999] as used by *Matthews et al.* [2005a], and observed atmospheric CFC and $\Delta^{14}C$ concentrations from OCMIP [*Orr et al.*, 1999].

[10] Figure 2a shows that the observed global mean surface air temperature increase during the 20th century is well reproduced by the model. The simulated global mean ocean temperature increase of 0.03°C from 1955 to 1998 (not shown) agrees well with the observed warming of 0.037°C [*Levitus et al.*, 2005]. Observations from the WOA01, which represent data from 1950 to 2000 will be compared with the model simulated tracer distributions

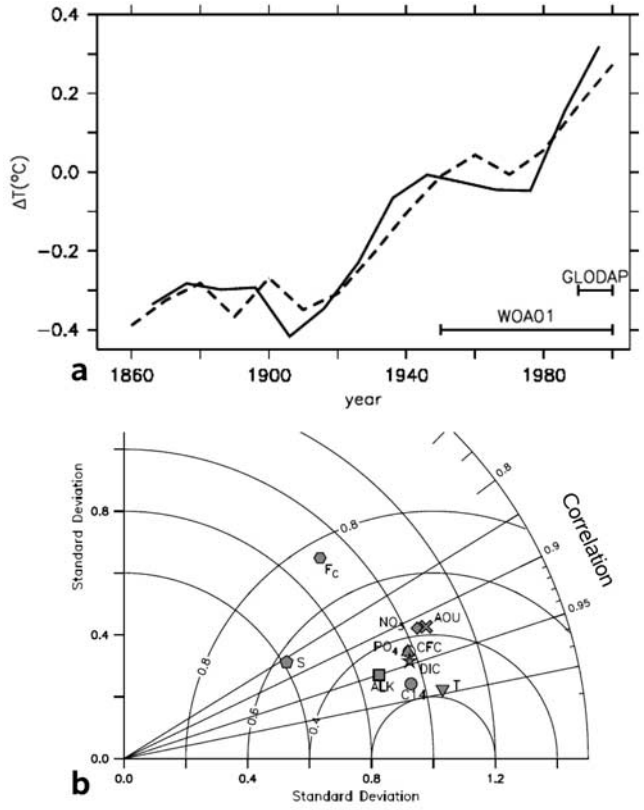

Figure 2. Comparison of model results with observations. (a) Observed (solid line) [*Jones et al.*, 2001] and simulated (dashed line) evolution of global surface air temperature anomaly (decadal mean) during the last 250 years. Bars in lower right corner show the period covered by the WOA01 (1950–2000) observations and that of the Global Data Analysis Project (GLODAP) [*Key et al.*, 2004] and *Takahashi et al.* [2002] data sets (1990–2000). (b) Taylor diagram [*Taylor*, 2001] of various global model fields compared with observations. All data are normalized with the standard deviation of the observations. Distance from the origin denotes the ratio of model standard deviation versus the observed. Correlation coefficient is given by the azimuth, and semicircular isolines centered around (1, 0) denote the pattern rms error. A perfect model with zero rms error, correlation coefficient of 1, and normalized standard deviation of 1 would plot at (1, 0). Note that the air-sea carbon flux F_C is a two-dimensional field in contrast to the other fields which are three-dimensional (3-D) and that its observational estimates [*Takahashi et al.*, 2002] have larger error bars than those of the 3-D fields.

averaged over the same time period. Observations from Global Data Analysis Project (GLODAP) [*Key et al.*, 2004] and the air-sea carbon fluxes represent average data from 1990 to 2000 and will be compared to the model results from this decade. The evaluation below focuses on the ocean biogeochemical cycles and ocean ventilation tracers since other model components have been evaluated previously in detail and the results are published elsewhere [*Weaver et al.*, 2001; *Meissner et al.*, 2003; *Schmittner et al.*, 2005a]. Figures 2b and 3 illustrates that the standard model simulates the observed present-day distribution of multiple tracers with skill. All tracers, except salinity and the air-sea flux of carbon, have correlation coefficients with the observations of more than 0.9 and pattern rms errors that are smaller than ~40% of the global standard deviation of the observations. The rms error for salinity, although worse than those for the other tracers, is typical for coarse resolution models. In fact, it is in the lower range of nine coupled models from international climate centers used in the upcoming 4th assessment report of the IPCC [*Schmittner et al.*, 2005b]. Basin-wide averaged vertical profiles of radiocarbon, CFCs, DIC and ALK are mostly within the error bars of the observations. Noticeable exceptions are too low DIC concentrations in the deep Indian and Pacific oceans and too high values in the Southern Ocean. ALK is underestimated in the deep Indian ocean. Basin-wide averages of temperature, salinity, phosphate, nitrate and apparent oxygen utilization (AOU = $O_2 - {}^{sat}O_2$, with ${}^{sat}O_2$ the temperature-dependent saturation concentration) appear to reproduce the main surface to deep and interbasin gradients of the observations. However, no error estimates are available for these tracers, precluding statements on the consistency of the model with the observations.

[11] Despite the relatively poor agreement of the air-sea carbon flux with observations implied by in Figure 2b, closer inspection shows that the model reproduces qualitatively and quantitatively most features of the observed global patterns (Figure 4) and that it is much improved compared to an earlier inorganic model version [*Ewen et al.*, 2004]. These features include outgassing at low latitudes with a maximum in the eastern tropical Pacific and in the Bering Sea, and uptake at mid and high latitudes with maxima around 45°N/S in the areas of the Gulf Stream and Kuroshio Current and in the Southern Ocean. Model biases include underestimated uptake in the Nordic Seas (caused by excessive sea ice cover) and in the South Atlantic, and underestimated outgassing in the Arabian Sea.

[12] Figure 5 shows the distribution of DIC and ALK in more detail. Generally, the simulated patterns show good agreement with observations. Noticeable features of the DIC distribution captured by the model include the surface to deep gradients as well as interbasin gradients in the deep ocean, with lower values in the Atlantic and maxima in the North Pacific and Indian Ocean. The amplitude of these maxima is underestimated by about 50 μmol/kg the model. Part of this underestimation is due to too weak stratification in the North Pacific in this model version. In a model with a stronger halocline the bias in the North Pacific is reduced to about 30 μmol/kg [*Schmittner et al.*, 2007b], which is still more than the error in the observations there (~10 μmol/kg). This, and slightly overestimated DIC (by ~15 μmol/kg) in the deep Southern Ocean, are the main remaining systematic model biases. The ALK distribution is similarly well captured by the model, including vertical and interbasin gradients. The largest differences occur in subtropical Atlantic surface waters which have too low ALK values by ~70 μmol/kg in the model. This is caused by deficiencies in the atmospheric

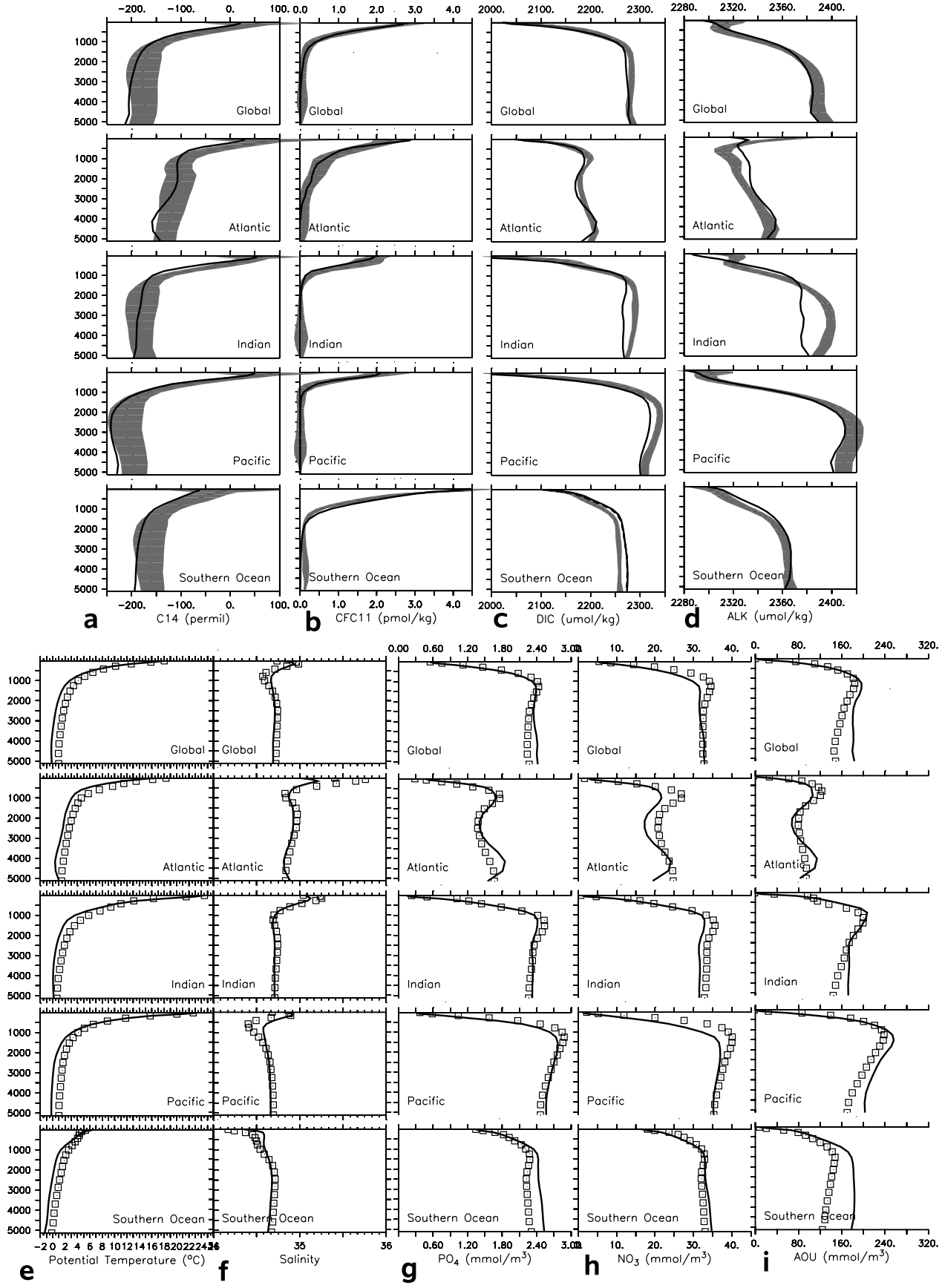
Global
Atlantic
Indian
Pacific
Southern Ocean
a
C14 (permil)
b
CFC11 (pmol/kg)
c
DIC (umol/kg)
d
ALK (umol/kg)
e
Potential Temperature (°C)
f
Salinity
g
PO4 (mmol/m3)
h
NO3 (mmol/m3)
i
AOU (mmol/m3)

Figure 3

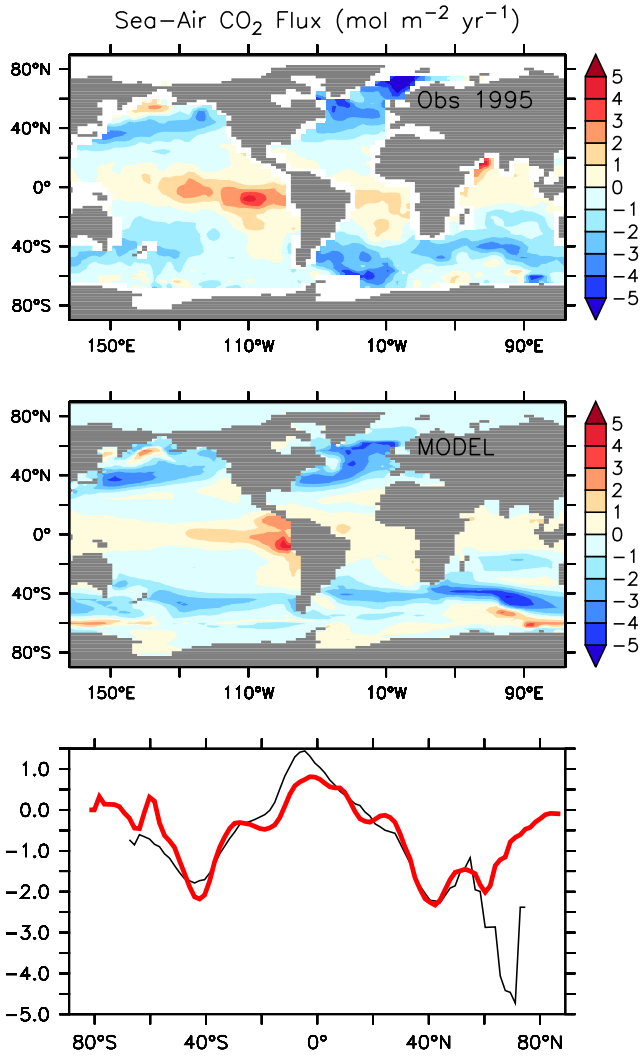

Figure 4. Air-sea flux of carbon from observations (top and black line in bottom) [*Takahashi et al.*, 2002] and the model (middle and red line in bottom). (bottom) Zonally averaged values as a function of latitude.

hydrological cycle as also evident in underestimated salinities there (not shown).

[13] Figure 6a shows depth distributions of CFC11. The generally excellent agreement with the observations suggests that ventilation of the upper and intermediate ocean on multidecadal timescales is well represented in the model. The largest model bias is underestimated Antarctic Bottom Water (AABW) formation, particularly in the Indian Ocean sector of the Southern Ocean. Too weak AABW production also explains overestimated phosphate and AOU values in the Southern Ocean (Figures 3g and 3i). A single core of North Atlantic Deep Water (NADW) is simulated in the model whereas a dual core of upper NADW and lower NADW is noticeable in the observations. Note that the difficulty of simulating the observed dual core structure of NADW seems to be a general problem in present coarse resolution models (none of nine models that submitted data to the IPCC AR4 analyzed by *Schmittner et al.* [2005b] is able to simulate this feature, not shown). Basin-wide profiles of simulated CFC11 are within the error bars of the observations for all basins and depths except in the deepest layers of the Southern Ocean where AABW formation seems to be slightly underestimated by the model. The simulated global inventory of 5.6×10^8 mol is consistent with the observations $(5.2 \pm 0.7) \times 10^8$ mol [*Matsumoto et al.*, 2004].

[14] The model also captures the observed ventilation of the deep ocean on centennial and millennial timescales as shown in Figure 6b in the radiocarbon fields. The vertical and interbasin gradients are, again, similar to observations. Simulated C14 fields are slightly too old (negative) everywhere presumably indicating too slow air-sea gas exchange. Deep water in the North Pacific is slightly too old in the model but is mostly within the error bars of the observations (not shown). Simulated radiocarbon values of deep water in the North Atlantic (−101‰), North Pacific (−240‰) and Southern Ocean Circumpolar Deep Water (−185‰) are within the 2σ error bars of the observations (−70 ± 50‰, −230 ± 25‰, −160 ± 25‰) considering the metric and deep water mass definitions proposed by *Matsumoto et al.* [2004]. The simulated global anthropogenic carbon inventory in the ocean during the 1990s is with 96 GtC slightly lower than the observational estimates of 118 ± 19 GtC [*Sabine et al.*, 2004]. In the Indo-Pacific north of 40°S the modeled inventory is 41 PgC, south of 40°S it is 18 PgC. Both numbers are consistent within the errors of observational estimates [*Matsumoto et al.*, 2004]. We conclude that the model is consistent with all metrics proposed by *Matsumoto et al.* [2004].

[15] The observed increase in atmospheric pCO_2 since 1800 is well reproduced (Figure 7) by our model as well as the partitioning of anthropogenic carbon between the different reservoirs at different times (Table 1). This represents an integral test of the coupled carbon cycle model. The agreement of the model with the observed oceanic and atmospheric inventories of anthropogenic carbon implies that the terrestrial uptake is also well captured.

4. Simulations of Future Climate

[16] Figure 8a shows the CO_2 emission scenario used to force the model. It is based on the SRES A2 nonintervention scenario until the year 2100 and subsequently a linear decline to zero at year 2300. The SRES A2 scenario represents a differentiated world with high population growth and moderate and uneven economic growth [*Nakicenovic et al.*, 2000]. Note that the current (2005) emissions (star in Figure 8a) of about 8 GtC/a are already about 30% of its peak emissions of 29 GtC/a in

Figure 3. Global and basin-wide averaged vertical profiles of various model tracers (solid lines) compared with observations. (a–d) Observations from GLODAP are shown as gray shaded areas including the published errors. (e–i) Observations from the WOA01 are shown as square symbols. Error estimates for these data are not available. Vertical axes denote depth in meters.

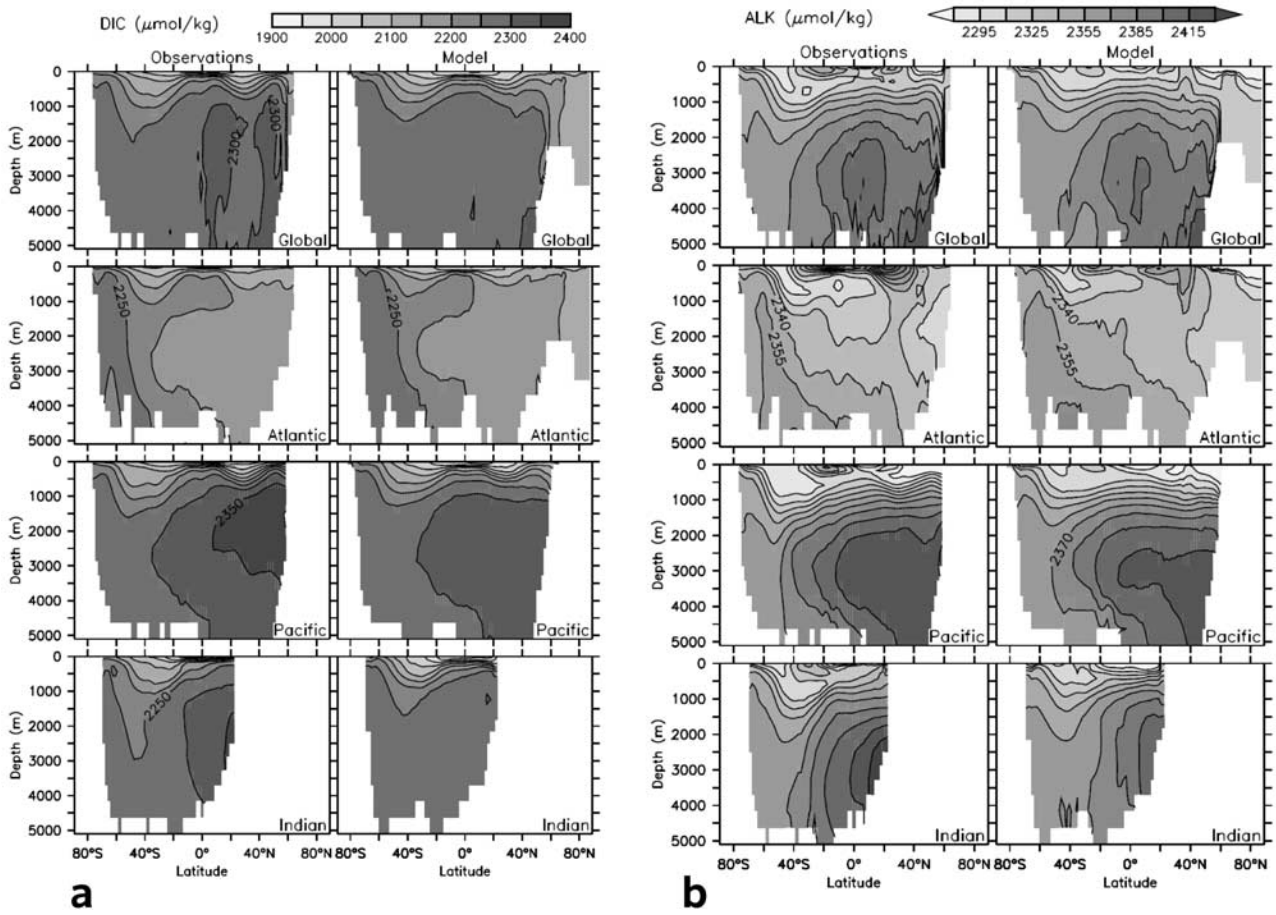

Figure 5. Zonally averaged distribution of dissolved inorganic carbon (DIC) (a) and alkalinity (ALK) (b) during the 1990s in the observations from GLODAP (left) and in the model (right). (top to bottom) All oceans, Atlantic, Pacific, Indian.

year 2100 and that emissions in recent years have been following this scenario rather than a stabilization scenario. In order to estimate the climate–carbon cycle feedback an additional simulation has been carried out with the same carbon emissions but in which changing atmospheric CO_2 concentrations do not affect the radiation balance at the top-of-the-atmosphere and hence climate, following the approach of *Friedlingstein et al.* [2003]. In this simulation, shown as dashed lines in Figures 8–9 and referred to as the constant climate run (CCR) in the following, the climate is almost unchanged although minor warming, of $<1^{\circ}$C, is caused by the physiological effects of rising ambient CO_2 concentrations on vegetation and associated changes in land surface albedo. The simulation with changing climate is referred to as the *fully coupled run* (FCR).

[17] In order to quantify the effect of biological carbon cycling the experiment including climate change has been repeated with a model version without ocean biology. In this model version the solubility pump is included only. The solubility pump is the enrichment of DIC in the deep ocean owing to higher CO_2 solubility of colder water. This experiment is referred to as the *no biology run* (NoBio).

4.1. Carbon Cycle

[18] Atmospheric CO_2 concentrations quickly rise and peak around year 2300 at values of more than 2000 ppmv in the fully coupled run (Figure 8a). Subsequently atmospheric CO_2 levels slowly decline to about 1700 ppmv at year 4000. These are much higher atmospheric CO_2 levels than in previous simulations with simpler models but similar emission scenarios. *Archer et al.* [1998] in their "A23" scenario using slightly less cumulative emissions of 4550 GtC predict atmospheric CO_2 levels of only $\sim$1000 ppmv around year 4000. *Lenton et al.* [2006] in their scenario "C", which has 4000 GtC total emissions, predict atmospheric CO_2 levels around 1100 ppmv at year 3000. The airborne fraction (i.e., the fraction of anthropogenic emissions remaining in the atmosphere; see solid line with square symbols in Figure 8b, middle) in FCR increases from 43% in year 2000 to 61% in year 2100 and 72% in year 2300, after which it declines slowly to 60% at year 3000 and 56% at year 4000. In comparison, the airborne fraction in the "A23" scenario from *Archer et al.* [1998] at year 4000 is only 44% and that of scenario "C" from *Lenton et al.* [2006] at year 3000 is 35–47%.

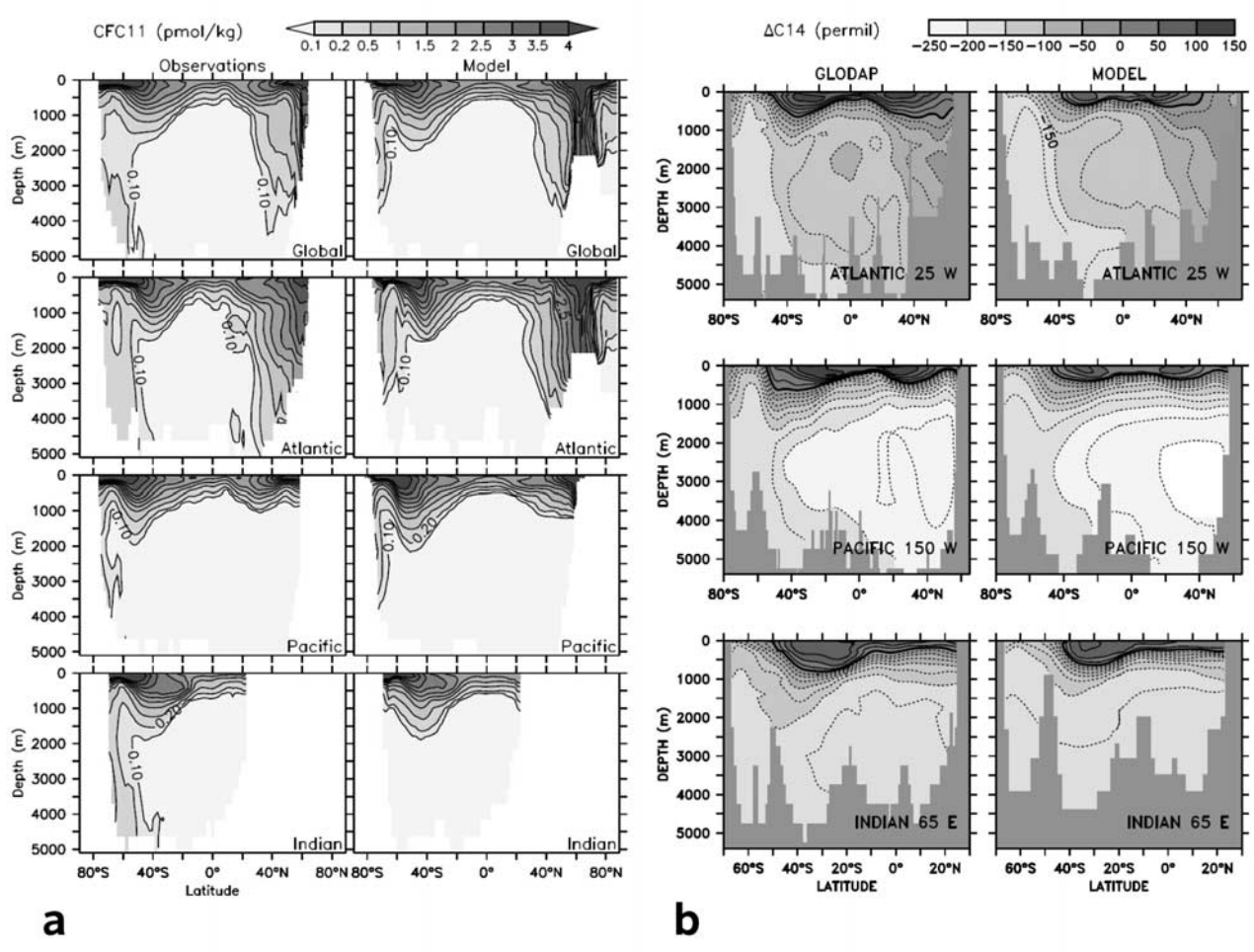

Figure 6. (a) As in Figure 5 but for CFC11. (b) Latitude-depth sections of radiocarbon.

[19] Note the delay of 100–200 years between the increase and peak in emissions and that of atmospheric CO_2 in our simulation (Figure 8a). Comparison with the CCR shows that climate–carbon cycle feedbacks, which are currently unimportant, quickly increase during the next few centuries and contribute 44% to the atmospheric CO_2 increase at year 4000 (Figure 8b, bottom). Vegetation and soil carbon pools on land, which have absorbed about 30% of cumulated anthropogenic carbon emissions up to now, become saturated around year 2100 and by year 2200 contain less than 10% of anthropogenic emissions. In the CCR land carbon uptake continues about 200 years longer until at year 2300 both soil and vegetation carbon increased each by about 460 Gt (not shown) amounting to about 20% of anthropogenic emissions (Figure 8b). In the FCR, vegetation uptake is reduced to 340 GtC and, more dramatically, soil carbon uptake has collapsed to only 40 Gt above preindustrial (not shown), because of a combination of accelerated soil respiration (which doubles by the year 4000 relative to 1800) and decreased vegetation carbon inputs from a climate-driven suppression of photosynthesis in the tropics [*Matthews et al.*, 2007]. Ocean uptake of

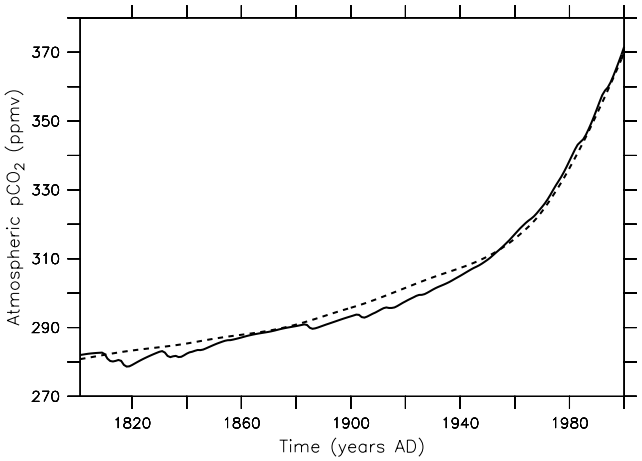

Figure 7. Annual mean atmospheric pCO_2 as simulated by the model (solid line) forced with carbon emissions compared to the observations (dashed line).

Table 1. Carbon Budget for the 1980s, 1990s, and 2000–2005 and Total Change From 1850 to 1998 (in GtC) From Model and Other Independent Estimates[a]

		1980s	1990s	2000–2005	1850–1998
Atmospheric increase	model	3.0	3.7	4.2	166.2
	estimate	3.3 ± 0.1[b]	3.2 ± 0.1[b]	4.1 ± 0.1[b]	176 ± 10[c]
Ocean uptake	model	−1.8	−2.1	−2.5	−104
	estimate	−1.8 ± 0.8[b]	−2.2 ± 0.4[b]	−2.2 ± 0.5[b]	−120 ± 50[d]
Terrestrial uptake	model	−2.6	−2.7	−2.5	−136
	estimate	−1.7 (−3.4 to 0.2)[b]	−2.6 (−4.3 to −0.9)[b]	NA	−126 ± 80[e]
Land use emissions	model	2.0	2.2	2.1	152
	estimate	1.3 (0.4–2.3)[b]	1.6 (0.5–2.7)[b]	NA	NA
Net terrestrial flux	model	−0.6	−0.5	−0.4	+16
	estimate	−0.3 ± 0.9[b]	−1.0 ± 0.6[b]	−0.7 ± 0.5[b]	NA

[a]Note that for the time period of 2000–2005 we assumed a constant shortwave forcing determined as the decadal average from 1988–1998 [from *Crowley*, 2000]. Units are GtC/a.
[b]From *IPCC* [2007, Table 7.1].
[c]From *Bolin et al.* [2000].
[d]From *Plattner et al.* [2002].
[e]From *Houghton* [2003].

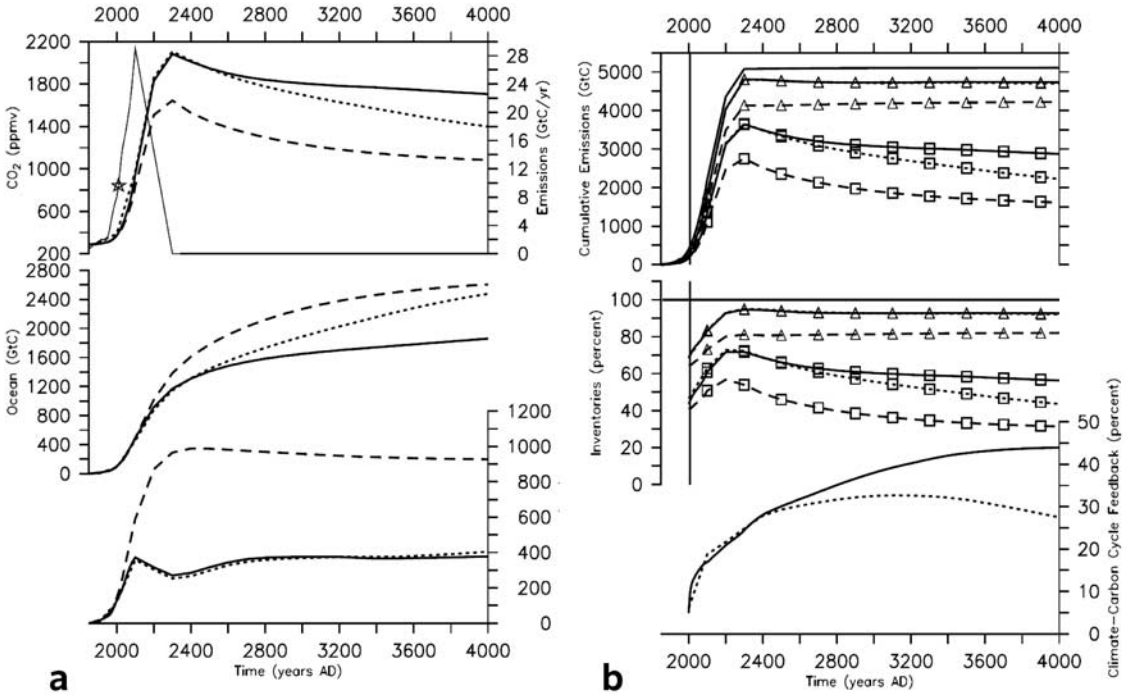

Figure 8. Simulated changes in carbon inventories. Solid lines correspond to the fully coupled model, dashed lines to a model with approximately constant climate (see text), and dotted lines correspond to a model without the ocean biological carbon cycle (NoBio). Differences between the solid and dashed lines indicate the climate–carbon cycle feedback, and the differences between the solid and dotted lines are caused by ocean biology. (a) (top) Carbon emissions (thin line) and atmospheric CO_2 concentration (thick line); star represents current (2005) emissions; (middle) ocean carbon uptake; (bottom) land carbon uptake. (b) (top) Total cumulative carbon emissions (solid line), atmospheric carbon uptake (squares), atmosphere plus ocean uptake (triangles). Land uptake can be inferred from the difference between the lines with triangles and the solid line; the ocean uptake is the difference between the lines with squares and the ones with triangles. (middle) Same as Figure 8b, top, but expressed as percentage of total emissions. Squares denote the airborne fraction, the difference between squares and triangles represent the sea-borne fraction, and the difference between triangles and the 100% line is the land-borne fraction. (bottom) Percentage atmospheric CO_2 increase due to the climate–carbon cycle feedback: (solid line) $(1 - \Delta pCO_2(CCR)/\Delta pCO_2\ (FCR))$, where ΔpCO_2 is the difference in atmospheric pCO_2 from preindustrial levels; (dotted line) $(1 - \Delta pCO_2(CCR)/\Delta pCO_2(NoBio))$.

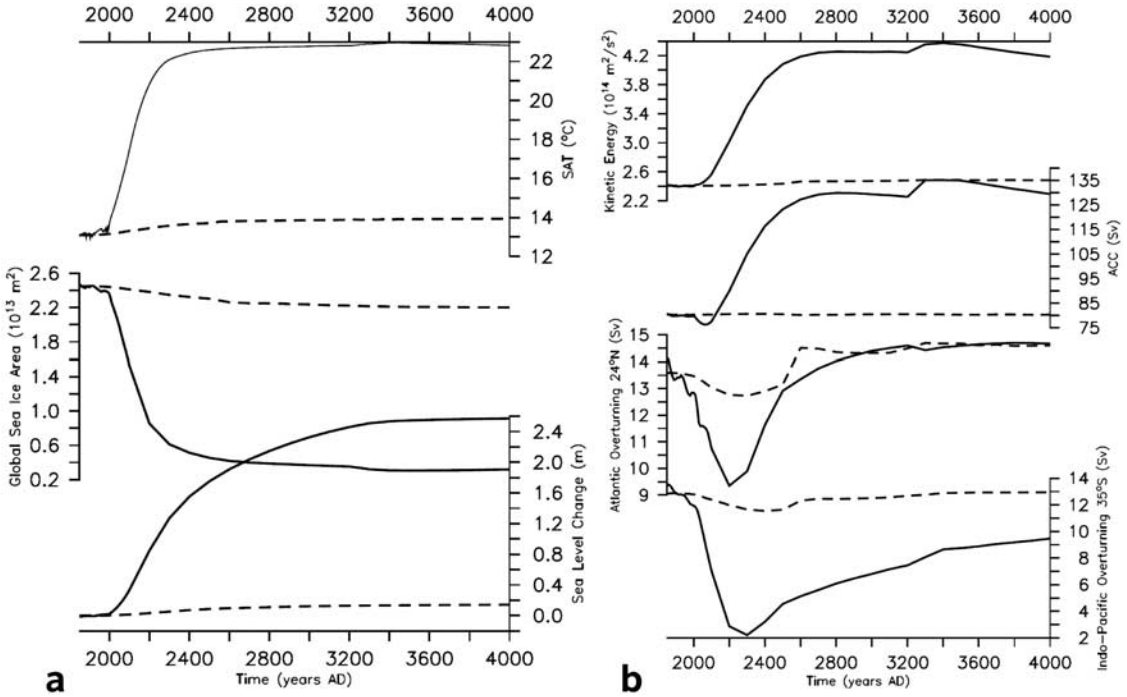

Figure 9. Simulated changes in climate and ocean circulation for the fully coupled (solid lines) and constant climate (dashed lines) runs. (a) (top) Surface air temperature (SAT); (middle) global sea ice area; (bottom) sea level change due to thermal expansion. Note that melting of glaciers is not considered in this estimate of sea level change. (b) (top to bottom) Global ocean kinetic energy, strength of Antarctic Circumpolar Current (ACC), Atlantic meridional overturning at 24°N, and inflow of Circumpolar Deep Water into the Indian and Pacific oceans.

anthropogenic carbon continues much longer than that on land, but is strongly reduced by climate change (by about 30% at year 4000, from 2606 Gt in the CCR to 1859 Gt in the FCR; Figure 8a, middle). Changes in the biological pump become important after year 2500 and are responsible for most of this reduction at year 4000.

[20] Our estimate of the climate–carbon cycle feedback (i.e., the change in atmospheric CO_2 from preindustrial levels in the fully coupled model divided by the change in the constant climate model) increases on a multicentennial to millennial timescale. At year 2100 only 17% (111 ppmv = 225 GtC) of the CO_2 increase is due to climate–carbon cycle feedbacks, within the range of previous estimates of 10–30% [*Cox et al.*, 2000; *Friedlingstein et al.*, 2003, 2006], but at year 2300 it is already 24% (438 ppmv = 886 GtC) and at year 3000 it is 38% (576 ppmv = 1164 GtC). This slow increase is due to changes in ocean biological carbon cycling which, in our model, are negligible before year 2500 but increase in importance until year 4000 at which they account for 37% of the total climate–carbon cycle feedback.

4.2. Climate and Ocean Circulation

[21] Because of the strong warming in the fully coupled model, global sea ice area collapses rapidly to less than 10% of its current area (Figure 9a). Temperatures at the sea surface and subsurface rise by 6–7°C at low latitudes to ~10°C at high latitudes (Figure 10). The deep sea warms by 2–5°C implying sea level rise by thermal expansion alone of 2.5 m (Figure 9a). The ocean circulation generally intensifies as shown by the integrated mean kinetic energy, which almost doubles (Figure 9b). This is mainly caused by an acceleration of the Antarctic Circumpolar Current (ACC) from 80 to 130 Sv owing to increased meridional pressure

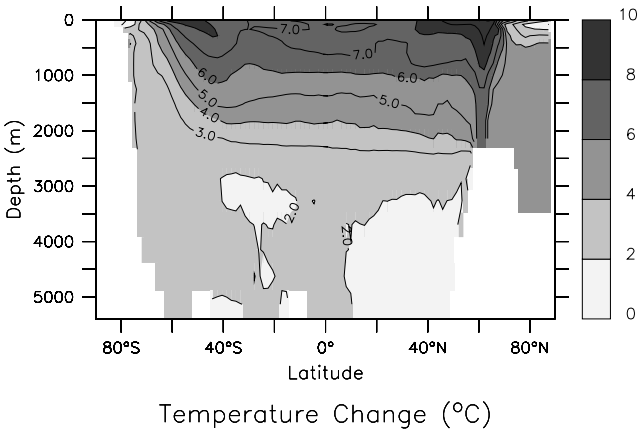

Figure 10. Zonally averaged difference in ocean potential temperature at year 4000 between fully coupled and constant climate simulations.

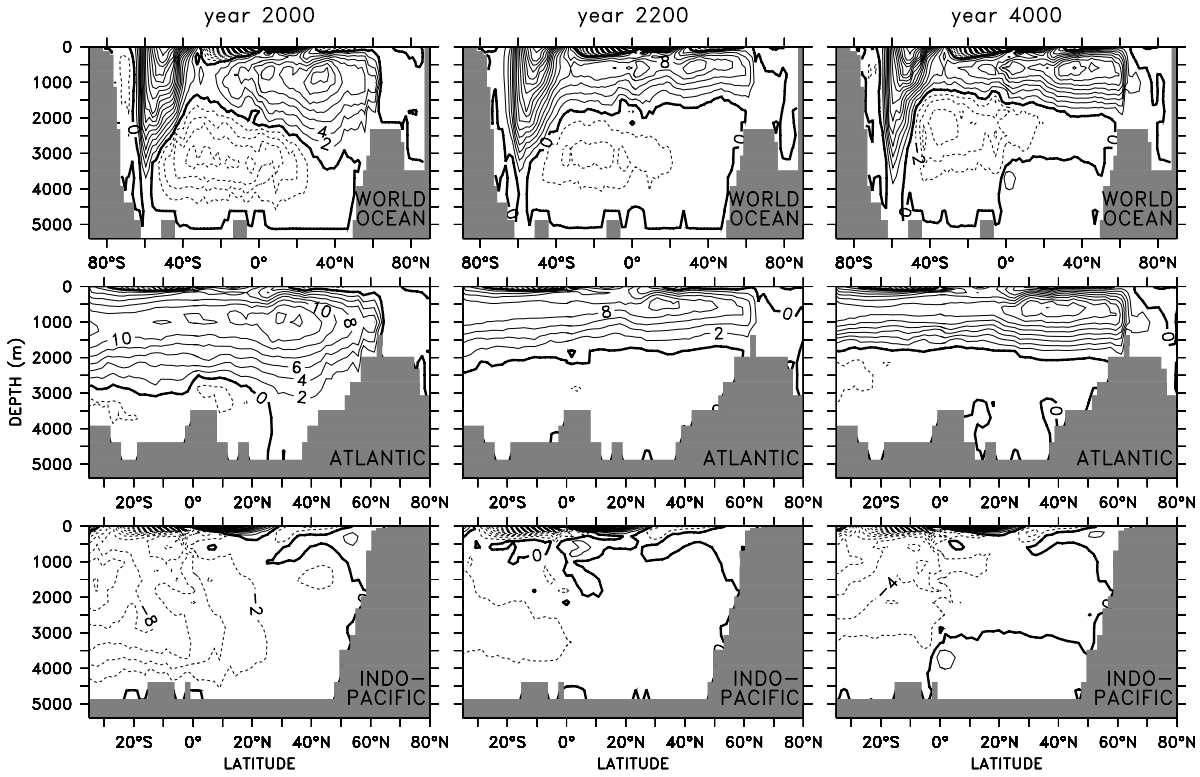

Figure 11. Meridional overturning stream function (Eulerian) in the world ocean (top), Atlantic (middle), and Indo-Pacific (bottom) at year 2000 (left), year 2200 (middle), and year 4000 (right). Flow is clockwise along isolines with positive values (solid lines) and anticlockwise for negative values (dashed lines). Isoline difference is 2 Sv.

gradients across the Southern Ocean that arise from greater warming at middle to low latitudes than in high-latitude waters around Antarctica (Figure 10). A strengthening of the ACC has recently been observed and attributed, at least in part, to human induced global warming and an associated southward shift and acceleration of zonal winds over the Southern Ocean [*Fyfe and Saenko*, 2005]. *Russell et al.* [2006] also find a strengthening of the ACC in global warming scenarios until year 2300, which they also attribute to a strengthening and southward shift in Southern Hemisphere westerly winds. In our simulation wind stress is held constant. Thus the accelerated ACC is not caused by wind stress changes but rather by an increase in the meridional density and pressure differences. Together these results imply that both wind and buoyancy forcing lead to a strengthening of the ACC in a warmer climate. It is therefore possible that part of the ACC increase found in the multicentennial simulations by *Russell et al.* [2006] is also caused by buoyancy forcing. The increase of the ACC simulated here (Figure 9b) has to be regarded as a lower limit because of the neglect of wind changes.

[22] The modeled deep overturning circulation slows down because of surface buoyancy input (Figure 11). Southward flow of North Atlantic Deep Water at 24°N decreases by as much as 30% at 2200, in agreement with the multimodel projections by *Schmittner et al.* [2005b], but recovers to its preindustrial strength by year 2700 although at a shallower depth (Figure 11). Note that melting of continental ice (e.g., Greenland) and consequent freshening of the North Atlantic is not included here nor in the IPCC AR4 simulations used by *Schmittner et al.* [2005b]. Although two recent model studies that try to estimate the effect of the melting of Greenland on the Atlantic overturning come to quite different conclusions on its magnitude [*Swingedouw et al.*, 2006; *Jungclaus et al.*, 2006], it is safe to say that melting of Greenland leads to an additional reduction of the circulation. Hence our projection represents a lower limit. More dramatic than the response of North Atlantic Deep Water is the reduction of Circumpolar Deep Water inflow into the Indian and Pacific oceans, which collapses from 14 Sv at year 1850 to 2 Sv at year 2200. This indicates a large reduction of Antarctic Bottom Water formation caused by reduced sea ice formation and freshening at high southern latitudes (sea surface salinity decreases by more than 1 salinity unit by year 2200). Higher water vapor content in a warmer atmosphere (the Clausius-Clapeyron relation) leads to increased poleward moisture transport and hence increased precipitation at high latitudes. Sea ice formation around Antarctica and its subsequent northward wind driven transport, which at present leads to brine rejection, salinification and bottom water formation around Antarctica [*Saenko et al.*, 2002], is also strongly reduced in the warm climate leading to a reduced mass flux of Antarctic Bottom Water. The subsequent recovery of the

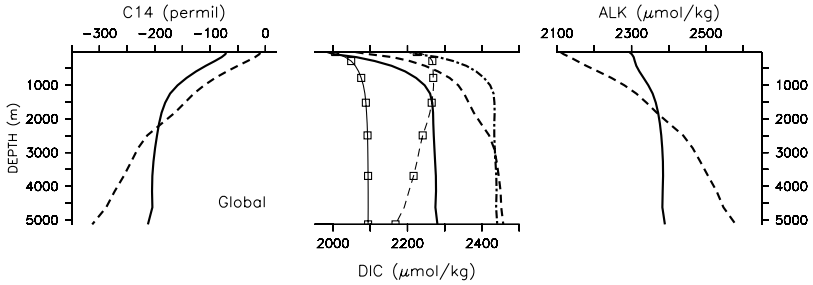

Figure 12. Global averaged profiles of radiocarbon, DIC, and ALK for the preindustrial simulation (year 1850, solid lines) and the end of the fully coupled run (year 4000, dashed lines). Dash-dotted line is from the fixed climate run. Thin lines with square symbols denote the model without ocean biology. Alkalinity profiles in the fixed climate run are almost identical as in the preindustrial simulation and therefore not visible.

deep circulation in the Indian and Pacific oceans is much slower than that of North Atlantic Deep Water and not complete by year 4000.

[23] Increased isolation of the deep sea from the atmosphere is also apparent in the radiocarbon distribution (Figure 12). Atmospheric $\Delta^{14}C$ is about 55 per mil higher than preindustrial and in the deep ocean it is more than 100 per mil lower. This translates to simulated bottom water ages in the North Pacific of more than 3500 years, in contrast to 2000 years today.

4.3. Ocean Ecosystem and Biogeochemical Cycling

[24] Increasing temperatures lead to faster recycling rates in the marine ecosystem (via equations (A10), (A14), and (A16) in Appendix A). Global primary production is boosted to almost double its preindustrial values (Figure 13). In the current model formulation, the acceleration of biological cycling in the upper ocean also leads to increased $CaCO_3$ production (see equation (3)) and hence a strongly increased alkalinity gradient (Figure 12). As a result of the different treatment of export of particulate organic and inorganic carbon (organic carbon sinks with finite sinking speed and remineralizes faster in a warmer ocean, whereas calcium carbonate is instantaneously exported to greater depths and remineralized according to a temperature-independent profile, see equation (4)), the globally averaged rain ratio doubles from 0.097 to 0.190. This increase in the rain ratio contributes to the positive climate–carbon cycle feedback because higher $CaCO_3$ production in the upper ocean increases the pCO_2 of surface waters and hence atmospheric

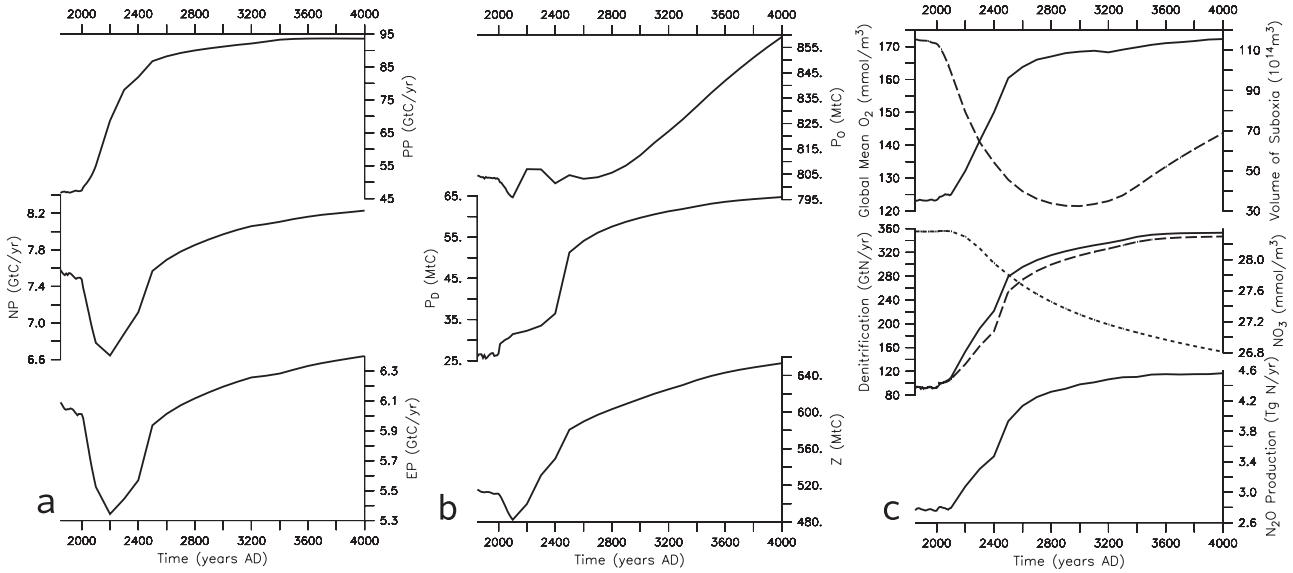

Figure 13. Time series of ocean biogeochemical variables. (a) (top) Net Primary Production (PP); (middle) New Production (NP); (bottom) Export Production by sinking particles (EP). (b) (top) Biomass of other phytoplankton; (middle) nitrogen fixers; and (bottom) zooplankton. (c) (top) Global mean oxygen (dashed line) and volume of suboxic water (solid line); (middle) global denitrification (solid line), nitrogen fixation (dashed line), and global mean nitrate (dotted line); (bottom) global nitrous oxide production.

Table 2. Changes Between Years 4000 and 1850 in Atmospheric pCO_2 (ΔpCO_2^A), Surface Ocean pCO_2 (ΔpCO_2^O), and Approximate Contributions to ΔpCO_2^O From Projected Changes in Temperature (T), Salinity (S), DIC (D), and ALK (A)[a]

Experiment	ΔpCO_2^A	ΔpCO_2^O	T, S	D, A	T	S	D	A
Fully coupled	1420	1428	137	976	136	18	158	466
Fixed climate	798	754	9	729	9	2	702	7

[a]The contribution of a given variable is calculated by comparing the ΔpCO_2^O using the surface ocean output for that variable at year 4000 and other state variables from year 1850 to the ΔpCO_2^O at year 1850. For example, the effect of temperature is calculated as pCO_2^O(T(t = 4000), S(t = 1850), DIC(t = 1850), ALK(t = 1850)) − pCO_2^O(T(t = 1850), S(t = 1850), DIC(t = 1850), ALK(t = 1850)). Changes in both temperature and salinity (T, S) and both DIC and ALK (D, A) are also shown. Note that because of nonlinearities in the pCO_2^O dependency the contributions of individual variables do not sum to the total change. Thus the numbers in this table are only useful to get an idea of the order of magnitude and importance of certain processes. For example, it can be concluded that salinity changes (S) have a negligible impact and that solubility effects alone (T) have a smaller effect than changes in dissolved inorganic carbon (DIC) and ALK. It is also clear that changes in alkalinity (ALK) are important in determining the fully coupled atmospheric CO_2 response, whereas in the fixed climate run they are negligible.

CO_2. To our knowledge this effect has not been suggested, described or considered before. We speculate, however, that common parameterizations of calcium carbonate production as a function of temperature-dependent primary production will yield similar results in other models. The comparison in Table 2 also confirms the important role alkalinity changes play in determining ocean surface and atmospheric pCO_2 in the FCR.

[25] The large increase of simulated primary production and $CaCO_3$ production is in sharp contrast to the response of new and export production (Figure 13), which both decline during the 21st and 22nd centuries by about 15% and recover afterward to values slightly higher than preindustrial. The transient decline is caused by the reduction in the overturning circulation during the same period, which impedes nutrient supply from upwelling as described by *Schmittner* [2005].

[26] Global phytoplankton stocks show surprisingly little response until about year 2800 after which they begin to increase gradually and reach about 5% higher values than preindustrial at year 4000. Zooplankton stocks increase more strongly by about 30% following the temperature rise. Both phytoplankton and zooplankton biomass show much larger changes regionally (Figure 14). They increase at high latitudes because of reduced sea ice cover and a longer growing season in agreement with earlier findings by *Bopp et al.* [2001]. North of about 55°N, plankton abundance increases in the North Atlantic because of deeper mixed layers and a northward shift in convections sites. In the northern Nordic Seas and Arctic ocean as well as around Antarctica stocks more than double by year 2400. Large relative increases in plankton mass are also simulated in the oligotrophic subtropical gyres. Faster nutrient recycling in the upper ocean allows more lateral advection of nutrients into these areas leading to a strong reduction in the area of oligotrophic oceans by year 4000. At mid latitudes both phytoplankton and zooplankton biomass decrease owing to increased stratification and reduced nutrient delivery into the photic zone. At year 2100 large reductions in phytoplankton stocks occur in the North Atlantic. In the Labrador and Irminger Seas as well as in the northeastern part of the subtropical gyre, in a broad band along the Iberian and northwest African margins biomass decreases by up to 50%. This is a response to the shoaling of mixed layers caused by the slow down of the Atlantic overturning circulation as shown earlier [*Schmittner*, 2005]. The ecosystem recovers there after year 2400. In the North Pacific plankton stocks decrease by about 20%. Nitrogen fixers migrate form the central tropical Pacific toward the east and move more than 15° poleward in both hemispheres owing to increased denitrification and warmer SSTs. Plankton abundance in the tropics shifts upward (not shown) from the subsurface level (80 m) to the surface (20 m) presumably due to more nitrate input from above (by nitrogen fixation) and less from below (enhanced denitrification).

[27] Warmer ocean temperatures lead to lower solubility of oxygen, which together with slower ventilation of the deep ocean lead to a ~30% decrease of global mean oxygen concentrations by year 3000 (Figure 13c). The oxygen changes are consistent with earlier 600-year model simulation using a simpler biogeochemical model [*Matear and Hirst*, 2002]. After year 3000, oxygen below 1 km depth slowly increases again because of the recovering deep ocean circulation (Figures 9b and 15a). Locally much larger reductions in oxygen concentrations are simulated. In the shallow subsurface ocean, for example (Figure 15b), oxygen concentrations decrease by more than 80% in the eastern equatorial Pacific and Atlantic. Along the West Coast of North America reductions of 40–80% occur. Such strong reductions in oxygen concentrations will very likely increase the frequency of hypoxic events on the shelves such as the ''dead zones'' on the Oregon shelf observed during the last few years [*Grantham et al.*, 2004]. The simulated volume of suboxic water triples by year 2500 and then remains constant (Figure 13c). This is accompanied by increased denitrification and, in turn, higher simulated nitrogen fixation since the ecological niche of nitrogen-fixing organisms (low-nitrate, high-phosphate waters) expands. Global stocks of nitrogen fixers more than double. The global average NO_3 concentration declines in our simulation by ~1.5 uM, or ~5%, although the magnitude of this decline is dependent on the ecological disadvantage that nitrogen fixers experience in the presence of nitrate, which is poorly quantified.

[28] It is well known that the oxygen minimum zones present an important source of nitrous oxide in the modern ocean [*Law and Owens*, 1990; *Yamagishi et al.*, 2005]. We estimate the effect of the simulated changes in oxygen concentrations and remineralization rates on the marine production of this potent greenhouse gas using equation (8)

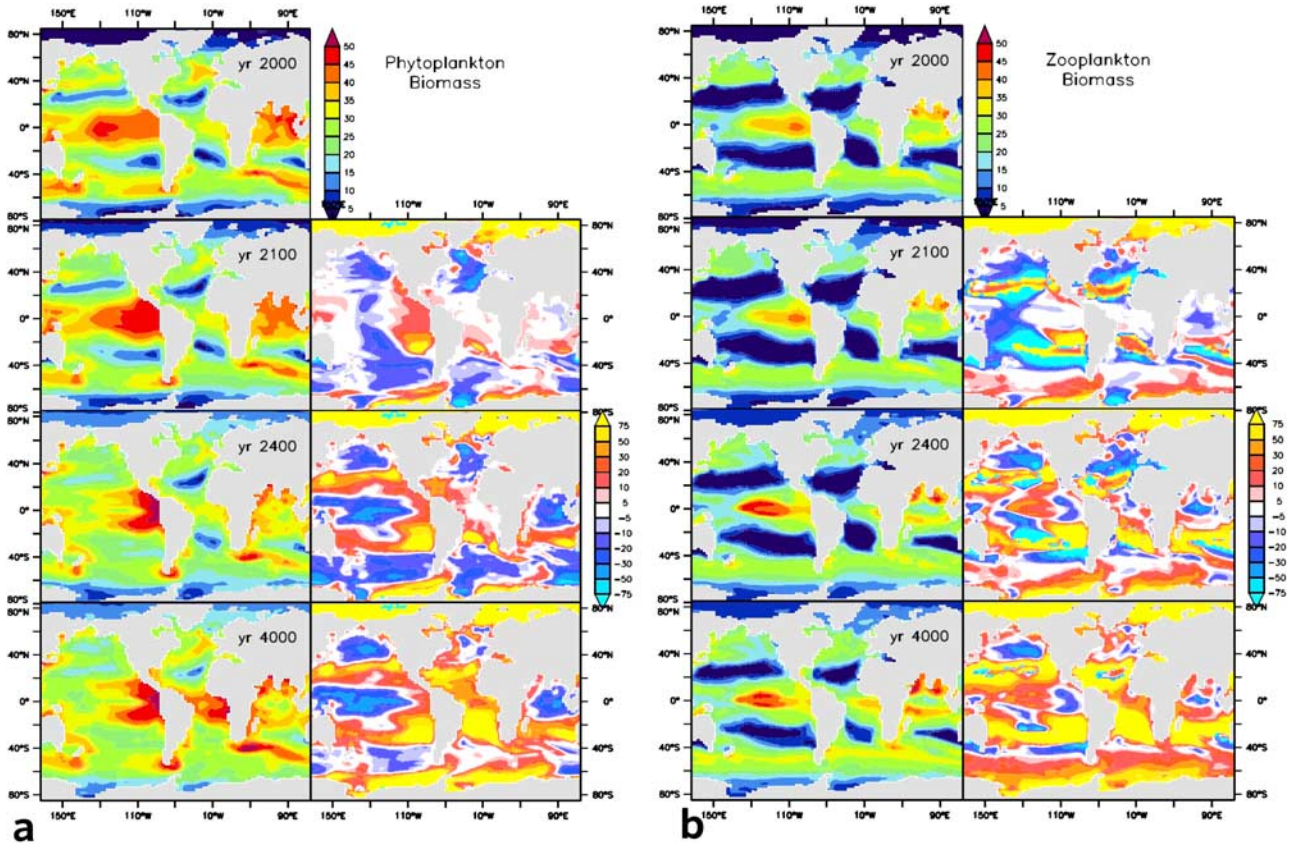

Figure 14. Snapshots of annually averaged, vertically integrated phytoplankton (a) and zooplankton (b) biomass. (left) Absolute values in units of mmol N/m^2. (right) Changes in percent from year 2000.

from *Nevison et al.* [2003]. As shown in Figure 13c, bottom, N_2O production increases by 64% owing to lower oxygen concentrations. Nitrification and denitrification, the main pathways of N_2O production, are both inhibited by oxygen [*Nevison et al.*, 2003]. Assuming a first-order sink in the stratosphere (the atmospheric lifetime of N_2O is about 120 years [*Prather et al.*, 2001]) and a constant land source of about the twice the size as the preindustrial ocean source [*Hirsch et al.*, 2006], yields an increase in atmospheric N_2O concentrations by about 21% or ~60 ppb. Calculating the radiative forcing (ΔF) of a 60 ppb increase of atmospheric N_2O concentrations from the preindustrial value of 270 ppb [*Flueckiger et al.*, 2004] according to *Ramaswamy et al.* [2001, Table 6.2] gives $\Delta F = 0.2$ W/m^2. Using a climate sensitivity $\alpha = \Delta T/\Delta F = 0.76$ K/(W/m^2) [*Annan and Hargreaves*, 2006], similar to that of the UVic model

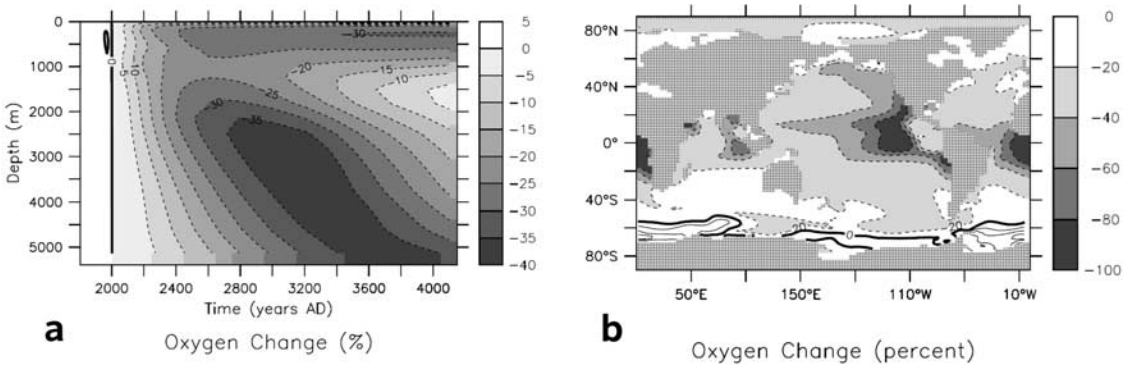

Figure 15. Percent oxygen changes between years 4000 and 2000. (a) Hovmoeller plot of global horizontally averaged changes. (b) Anomalies at 286-m depth.

($\sim$0.9 K/(W/m^2)), we can estimate the global mean warming due to this effect which amounts to $\Delta T = 0.2$ K. This is more than an order of magnitude smaller than the warming associated with the CO_2 release.

5. Discussion

[29] We have shown that our model has skill in simulating a large number of observational data sets from the past 50 years and that it is mostly consistent (within the error bars) with those observations that provide error estimates. However, this does not guarantee reliability of simulations of a climate that is very different from the one of today. Comparisons with proxy data of paleoclimates offer the opportunity to evaluate the fidelity of the model to reproduce climates much different from today's and/or more drastic climatic changes than those observed during the observations period (last 150 years). The physical model has been successfully applied earlier to simulations of the last glacial maximum [*Weaver et al.*, 1998; *Schmittner et al.*, 2002a; *Meissner et al.*, 2003] and rapid climate changes during the last ice age [*Schmittner et al.*, 2002b, 2003; *Clark et al.*, 2007]. These studies together with recent paleostudies using the ocean biogeochemical model [*Schmittner*, 2005; *Schmittner et al.*, 2007a, 2007b] suggest that the model has skill in simulating climates different from the one of today. However, a past analog for the future is lacking and quantitative comparison with the paleoproxy record is difficult. Therefore we believe that it is likely that the further the climate strays from that of today, the larger the errors in the simulation will become. Thus we do not claim that our results represent a realistic depiction of Earth's climate 10°C warmer than today. However, we believe that the model simulations, with the exception of the neglected changes in the wind field and glacier melting, are a self-consistent representation of possible future changes and that they might elucidate potentially important but so far overlooked feedback mechanisms operating on centennial to millennial timescales. Different aspects of the simulations will differ in their fidelity. Below we provide a more detailed discussion of the confidence that can be put in individual results and the uncertainties associated with them.

[30] The positive climate–carbon cycle feedback increases over a multimillennial timescale because of changes in ocean carbon cycling that exceed those estimated by previous, shorter simulations [*Friedlingstein et al.*, 2006]. Our simulated atmospheric CO_2 levels are also much larger than those from earlier millennial timescale studies using simpler models but similar emission scenarios [*Archer et al.*, 1998; *Lenton et al.*, 2006]. Changes in the biological pump are unimportant until 2600 but subsequently strengthen to account for most of the ocean component of the climate–carbon cycle feedback at year 4000. Central to this feedback is an increase in calcium carbonate production associated with higher primary production and accelerated biological activities in warmer sea water. Note that this effect, which is biological, is different from the chemical effect of increasing surface ocean pCO_2 on the ratio of released CO_2 to precipitated carbonate [*Frankignoulle et al.*, 1994].

[31] Our model response clearly depends on the formulation used to compute the temperature dependency of biological rates. Here we used the widely applied exponential function from *Eppley* [1972]. Note that maximum simulated SSTs in our global warming experiment are around 36°C (Figure 10) and thus well within the range of data used by Eppley (his data go up to 40°C). However, it is not clear whether the Eppley curve is universally applicable to both growth and respiration. Individual species have, through the evolutionary process, adapted to a certain climate regime and their growth rates follow a curve with a maximum at the optimum temperature and lower values at warmer and cooler temperatures. It is possible that the Eppley curve holds for an average of many different species with different optimum temperatures [*Moisan et al.*, 2002], however it is not certain that this will also be the case for particular plankton functional types. It will therefore be important to use a more detailed ecosystem model with different plankton types that distinguishes between calcifiers and non calcifying organisms in order to test whether our results are robust. Such a model requires a parameterization of the temperature dependence of growth rates of calcifiers as a plankton functional group based on measurements.

[32] At this point we believe that the agreement of our simulated rain ratios with observational estimates under today's climate conditions (Figure 1) provides some support for the temperature dependency of calcium carbonate versus particulate (soft tissue) organic matter production that follows from the application of the Eppley curve. We note, however, that this good agreement may be fortuitous and that better and more mechanistic models of calcium carbonate production, sinking and dissolution will be needed to clarify this issue. Note also that the ocean primary production increase until 2050 predicted by our model (4 GtC or 8%) is consistent with, but on the higher end of the range (0.7–8.1%) of the independent projections by *Sarmiento et al.* [2004]. The latter authors also stress the importance of the temperature dependence of primary production algorithms. Here we reemphasize the need for more research and experimental data on the temperature dependency of maximum growth rates as well as other biological rates such as fast microbial recycling and remineralization of particulate organic matter, given their tremendous importance for the Earth's long-term future. This issue also affects our simulated changes in plankton biomass (Figure 14), which, for the same reasons, should be regarded as preliminary.

[33] We did not consider effects of upper ocean acidification on calcification. CO_2 infusion reduces the pH, the carbonate ion concentrations and hence the saturation levels of calcium carbonate in sea water. It has been shown that this has adverse effects on the calcification of marine organisms such as corals and certain plankton species [*Riebesell et al.*, 2000] although geological information on some calcifying algae suggests adaptation and insensitivity to changes in pH on longer timescales [*Langer et al.*, 2006]. Still, ocean acidification has the potential to reduce the rain ratio in the future [*Orr et al.*, 2005] and would counteract the effect of increased calcium carbonate production in warmer water. Different previous model studies tried to quantify the effect of ocean acidification on future ocean

carbon uptake and atmospheric CO_2 concentrations. *Heinze* [2004] isolated the effect of acidification by keeping climate constant in a scenario in which atmospheric CO_2 increased to 1400 ppmv until year 2250. He finds a reduction of the $CaCO_3$ production by one half but a decrease of atmospheric CO_2 by year 2250 of only 10 ppmv.

[34] An improved quantification of this effect including uncertainties in its parameterization [*Ridgwell et al.*, 2006] suggest higher future uptake of anthropogenic CO_2 and reduced atmospheric CO_2 levels at year 3000 of 30–100 ppmv. This amplitude is smaller but similar to the biological effects in our simulation (108 ppmv) at that time. Since both effects lead to changes with different signs, the net effect might be much smaller than our projections or the ones of *Ridgwell et al.* [2006].

[35] Note that our formulation of $CaCO_3$ production is different from the one used by *Ridgwell et al.* [2006], who assume it proportional to the export production of POM with a proportionality factor that considers the saturation state of surface waters with respect to $CaCO_3$. Their scheme also produces a latitudinal distribution with lower values at high latitudes and higher values at low latitudes in qualitative agreement with the observations. However, their rain ratios [*Ridgwell et al.*, 2006, Figure 5c] show maxima of 0.17 in the subtropics and local minima along the equator, apparently in conflict with the observational patterns (Figure 1). This, together with the better agreement of our simulated rain ratios with observations, suggests that at least part of the observed latitudinal distribution is explained by a temperature effect (that is not considered by *Ridgwell et al.* [2006]).

[36] In the as yet most complete parameterization, including effects of increased dissolution, *Gehlen et al.* [2007] using a 4 $\times$ CO_2 scenario, also show a large decrease in $CaCO_3$ production by 27%, but only a negligible effect on oceanic carbon uptake (6 GtC) and hence atmospheric CO_2. The reason(s) for the different effects of acidification on future oceanic carbon uptake in these three studies [*Heinze*, 2004; *Ridgwell et al.*, 2006; *Gehlen et al.*, 2007] are not clear. The small effect by *Heinze* [2004] and *Gehlen et al.* [2007] may be in part be due to the short integration time. As discussed in more detail by *Gehlen et al.* [2007], considerable uncertainties are associated with the parameterizations. Nevertheless, all three studies report consistently a decrease in the $CaCO_3$ production which would counteract the temperature effect described in this paper. The effect of ocean acidification on atmospheric CO_2 on long (longer than a few centuries) timescales, however, remains to be quantified.

[37] In our global warming simulations oxygen concentrations strongly decrease leading to accelerated water column denitrification. Whereas the global patterns of ocean oxygen concentrations are well captured in the model, difficulties remain in the simulation of suboxic zones. This is discussed in more detail by *Schmittner et al.* [2007a]. Briefly, low resolution and high meridional viscosities lead to an underestimation of zonal currents in the tropics such as the Equatorial Under Current [*Large et al.*, 2001]. Consequently, oxygen delivery to the eastern equatorial Pacific is too small and suboxic zones are too large in the model. This suggests that the simulation of denitrification and nitrogen fixation is less reliable than the general decrease in oxygen concentrations, which seems to be robust in different models [*Matear and Hirst*, 2002]. Furthermore, changes in wind driven ocean circulation, which is neglected in our simulations, will certainly lead to regional differences in the simulated oxygen changes [*Schmittner et al.*, 2007a]. Changes in wind driven circulation might also affect the climate–carbon cycle feedback, e.g., through changes in Southern Ocean ventilation [*Russell et al.*, 2006]. These effects remain to be quantified on multimillennial timescales.

6. Conclusions

[38] Our simulations suggest the positive feedback between climate change and the carbon cycle will continue to increase on a multicentennial to millennial timescale and that it may become larger than previous shorter model simulations suggested. A previously unconsidered feedback mechanism between temperatures and calcium carbonate production in the surface ocean strengthens the vertical alkalinity gradient, leading to reduced carbon uptake in a warmer sea. Changes in biological carbon cycling in the ocean have negligible impact on atmospheric CO_2 until about 2600. This suggests that shorter (century-scale) simulations can be carried out without ocean biology. On millennial timescales, however, changes in the biological pump contribute to a large fraction (37%) of the total climate–carbon cycle feedback and need to be taken into account. These estimates need to be taken with caution since they rely on the simulated changes in calcium carbonate production and do not take into account acidification and attendant changes in the carbonate chemistry. Our results demonstrate the importance that changes in $CaCO_3$ cycling can have on projected levels of future atmospheric CO_2 and climate. Improved, process based models of $CaCO_3$ production and dissolution are urgently needed in order to improve estimates of the effects of anthropogenic CO_2 emissions on millennial timescales.

[39] Warming and ventilation changes lead to lower oxygen concentrations and a large increase of denitrification in the water column in our simulations (Figure 13c). Production rates of nitrous oxide (N_2O), an important and potent greenhouse gas increase by 60%. This represents another positive feedback mechanism which we quantify for the first time. We estimate a radiative forcing of 0.32 W/m^2 which suggests that the amplitude of this feedback (ΔT = 0.24 K) is more than an order of magnitude smaller than the warming associated with CO_2.

[40] Taken together these results suggest that, unless action is taken soon in order to reduce the uncontrolled burning of fossil fuels, future generations will live in a very different world from the one we experience today. Even the complete elimination of fossil fuel use by year 2300 will not result in a return to the preanthropogenic state within the next several millennia, but Earth's climate will stabilize in an alternate mode, the nature of which is determined by the cumulative carbon emissions.

[41] The delay of more than 100 years between the emissions peak and the resulting peak of atmospheric CO_2

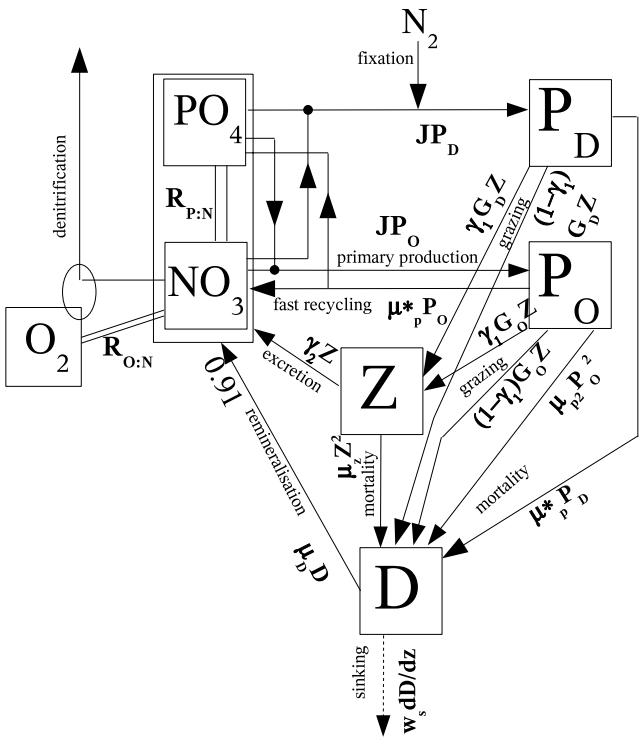

Figure A1. Ocean ecosystem model schematic. Different compartments (squares) are connected through the fluxes (arrows) as explained in detail in the text.

(Figures 8a and 9a) is a critical feature of our results. By year 2100 the year of peak emissions, atmospheric CO_2 will have increased by 580 ppmv above preindustrial levels and surface air temperatures will be 4°C warmer. Two hundred years later, when emissions have decreased to zero, atmospheric CO_2 is reaching its peak value of 1800 ppmv above preindustrial values and the climate is 8.4°C warmer. This delayed response of the climate system and carbon cycle indicates that CO_2 concentrations and temperatures will continue to rise for a long time after emission reductions are implemented. It follows that humans may commit the planet to dangerous climate change through emissions generated while the observed climate change remains still relatively mild [*Wigley*, 2005]. This is a treacherous situation and suggests that we cannot wait until climatic changes are so large that they strongly and directly affect our lives. Early action on emission reductions is needed in order to avoid dangerous climate change for future generations.

Appendix A: Description of Marine Ecosystem Model Component

[42] The marine ecosystem model (Figure A1) is an improved version of *Schmittner et al.* [2005a] and includes interactive cycling of nitrogen, phosphorus and oxygen. It is based on seven prognostic variables and embedded within the ocean circulation model. The inorganic variables include dissolved oxygen (O_2) and two nutrients, nitrate (NO_3) and phosphate (PO_4) which are linked through exchanges with the biological variables by constant (∼Redfield) stoichiometry (Table A1). The biological variables include two classes of phytoplankton, nitrogen-fixing diazotrophs (P_D), and other phytoplankton (P_O), as well as zooplankton (Z) and particulate detritus (D); all biological variables are expressed in units of mmol nitrogen per m^3. Although very simple, this ecological structure captures the essential dynamic of competition for phosphorus highlighted by *Tyrell* [1999], in which phytoplankton capable of rapid growth using available nutrients (P_O) are pitted against slow growers capable of fixing their own supply of nitrogen (P_D). Additional information on the nitrogen cycle is given by *Schmittner et al.* [2007a].

[43] Each variable changes its concentration C according to the following equation

$$\frac{\partial C}{\partial t} = T + S, \tag{A1}$$

where T represents all transport terms including advection, isopycnal and diapycnal diffusion, and convection. S denotes the source minus sink terms, which describe the biogeochemical interactions as follows:

$$S(\mathrm{PO_4}) = (\mu_D \mathrm{D} + \mu_P^* \mathrm{P}_O + \gamma_2 \mathrm{Z} - J_O \mathrm{P}_O - J_D \mathrm{P}_D) R_{P:N} \tag{A2}$$

$$S(\mathrm{NO_3}) = (\mu_D \mathrm{D} + \mu_P^* \mathrm{P}_O + \gamma_2 \mathrm{Z} - J_O \mathrm{P}_O - u_\mathrm{N} J_D \mathrm{P}_D) \cdot \left(1 - 0.8 R_{O:N}\, r_{sox}^{NO3}\right) \tag{A3}$$

$$S(\mathrm{P}_O) = J_O \mathrm{P}_O - \mu_P^* \mathrm{P}_O - G(\mathrm{P}_O)\mathrm{Z} - \mu_{P2} \mathrm{P}_O^2 \tag{A4}$$

$$S(\mathrm{P}_D) = J_D \mathrm{P}_D - G(\mathrm{P}_D)\mathrm{Z} - \mu_P \mathrm{P}_D \tag{A5}$$

$$S(\mathrm{Z}) = \gamma_1 [G(\mathrm{P}_O) + G(\mathrm{P}_D)]\mathrm{Z} - \gamma_2 \mathrm{Z} - \mu_\mathrm{Z} \mathrm{Z}^2 \tag{A6}$$

$$S(\mathrm{D}) = (1-\gamma_1)[G(\mathrm{P}_O) + G(\mathrm{P}_D)]\mathrm{Z} + \mu_P \mathrm{P}_D + \mu_{P2} \mathrm{P}_O^2 + \mu_\mathrm{Z} \mathrm{Z}^2 - \mu_D \mathrm{D} - w_\mathrm{D}\, \partial \mathrm{D} \partial z \tag{A7}$$

$$S(\mathrm{O_2}) = F_{sfc} - S(\mathrm{PO_4}) R_{O:P}\, r_{sox}^{O2} \tag{A8}$$

The function $J_O = J(I, \mathrm{NO_3}, \mathrm{PO_4})$ provides the growth rate of nondiazotrophic phytoplankton, determined from irradiance (I), NO_3 and PO_4,

$$J(I, \mathrm{NO_3}, \mathrm{PO_4}) = \min(J_{OI}, J_{O\max} u_N, J_{O\max} u_P), \tag{A9}$$

The maximum growth rate is dependent only on temperature (T):

$$J_{O\max} = a \times \exp(T/T_b) \tag{A10}$$

Table A1. Ocean Ecosystem and Carbon Cycle Model Parameters

Parameter	Symbol	Value	Units
Phytoplankton (P_O, P_D) Coefficients			
Initial slope of P-I curve	α	0.1	$(\mathrm{W\ m^{-2}})^{-1}\ \mathrm{d^{-1}}$
Photosynthetically active radiation	PAR	0.43	
Light attenuation in water	k_w	0.04	$\mathrm{m^{-1}}$
Light attenuation through phytoplankton	k_c	0.03	$\mathrm{m^{-1}(mmol\ m^{-3})^{-1}}$
Light attenuation through sea ice	k_I	5	$\mathrm{m^{-1}}$
Maximum growth rate	a	0.11	$\mathrm{d^{-1}}$
Half-saturation constant for N uptake	k_N	0.7	$\mathrm{mmol\ m^{-3}}$
Specific mortality rate	μ_P	0.025	$\mathrm{d^{-1}}$
Fast recycling term (microbial loop)	μ_{P0}	0.02	$\mathrm{d^{-1}}$
Diazotrophs' handicap	c_D	0.5	
Zooplankton (Z) Coefficients			
Assimilation efficiency	γ_1	0.925	
Maximum grazing rate	g	1.575	$\mathrm{d^{-1}}$
Prey capture rate	ε	1.6	$(\mathrm{mmol\ m^{-3}})^{-2}\ \mathrm{d^{-1}}$
Mortality	μ_Z	0.34	$(\mathrm{mmol\ m^{-3}})^{-2}\ \mathrm{d^{-1}}$
Excretion	γ_2	0.01	$\mathrm{d^{-1}}$
Detritus (D) Coefficients			
Remineralization rate	μ_{D0}	0.048	$\mathrm{d^{-1}}$
Sinking speed at surface	w_{D0}	7	$\mathrm{M\ d^{-1}}$
Increase of sinking speed with depth	m_w	0.04	$\mathrm{d^{-1}}$
E-folding temperature of biological rates	T_b	15.65	°C
Other Coefficients			
Molar elemental ratios	$R_{C:N}$	7	
	$R_{O:N}$	13	
	$R_{N:P}$	16	
	$R_{C:P}$	112	
$CaCO_3$ over nonphotosynthetical POC production ratio	$R_{CaCO3/POC}$	0.035	
$CaCO_3$ remineralization e-folding depth	D_{CaCO3}	3500	m

such that growth rates increase by a factor of ten over the temperature range of −2 to 34°C. We use $a = 0.11\ \mathrm{d^{-1}}$ for the maximum growth rate at 0°C which was determined to optimize surface nutrient concentrations. Under nutrient-replete conditions, the light-limited growth rate J_{OI} is calculated according to

$$J_{OI} = \frac{J_{O\max}\alpha I}{\left[J_{O\max}^2 + (\alpha I)^2\right]^{1/2}} \tag{A11}$$

where α is the initial slope of the photosynthesis versus irradiance (P-I) curve. The calculation of the photosynthetically active shortwave radiation I and the method of averaging equation (13) over 1 day is outlined by *Schmittner et al.* [2005a]. Nutrient limitation is represented by the product of $J_{O\max}$ and the nutrient uptake rates, $u_\mathrm{N} = \mathrm{NO_3}/(k_\mathrm{N} + \mathrm{NO_3})$ and $u_\mathrm{P} = \mathrm{PO_4}/(k_\mathrm{P} + \mathrm{PO_4})$, with $k_\mathrm{P} = k_\mathrm{N}R_{P:N}$ providing the respective nutrient uptake rates.

[44] Diazotrophs grow according to the same principles as the other phytoplankton, but are disadvantaged in nitrate-bearing waters by a lower maximum growth rate, $J_{D\max}$, which is zero below 15°C:

$$J_{D\max} = c_D \max[0, a(\exp(T/T_b) - 2.61)]. \tag{A12}$$

The coefficient c_D handicaps diazotrophs by dampening the increase of their maximal growth rate versus that of other phytoplankton with rising temperature. We use $c_D = 0.5$, such that the increase per °C warming of diazotrophs is 50% that of other phytoplankton. However, diazotrophs have an advantage in that their growth rate is not limited by $\mathrm{NO_3}$ concentrations:

$$J_D(I, \mathrm{PO_4}) = \min(J_{DI}, J_{D\max}u_P), \tag{A13}$$

although they do take up $\mathrm{NO_3}$ if it is available (see term 5 in the right-hand side of equation (A3)). The N:P of model diazotrophs is equal to other phytoplankton (16:1). Although there is evidence that the best-studied diazotrophs of the genus *Trichodesmium* can have much higher N:P [e.g., *Sanudo-Wilhelmy et al.*, 2004], the more abundant unicellular diazotrophs are uncharacterized [*Montoya et al.*, 2002] and for simplicity of interpretation we opted to keep the N:P of both phytoplankton groups identical.

[45] The first-order mortality rate of phytoplankton is linearly dependent on their concentration, P_O. DOM and the microbial loop are folded into a single fast remineralization process, which is the product of P_O and the temperature-dependent term

$$\mu_P^* = \mu_{P0}^* \exp(T/T_b). \tag{A14}$$

Diazotrophs do not undergo this fast remineralization, but die at a linear rate.

[46] Grazing of phytoplankton by zooplankton is unchanged from *Schmittner et al.* [2005a]. Detritus is generated from sloppy zooplankton feeding and mortality among the three classes of plankton, and is the only component of the ecosystem model to sink. It does so at a speed of

$$w_D = \left\{ \begin{array}{c} w_{D0} + m_w z, z \le 1000m \\ w_{D0} + m_w 1000m, z > 1000m \end{array} \right\}, \quad \text{(A15)}$$

increasing linearly with depth z from $w_{D0} = 7$ m d^{-1} at the surface to 40 m d^{-1} at 1 km depth and constant below that, consistent with observations [*Berelson*, 2002]. The remineralization rate of detritus is temperature dependent and decreases by a factor of 5 in suboxic waters, as O_2 decreases from 5 μM to 0 μM:

$$\mu_D = \mu_{D0} \exp(T/T_b)[0.65 + 0.35 \tanh(O_2 - 6)]. \quad \text{(A16)}$$

Remineralization returns the N and P content of detritus to NO_3 and PO_4. Photosynthesis produces oxygen, while respiration consumes oxygen, at rates equal to the consumption and remineralization rates of PO_4, respectively, multiplied by the constant ratio $R_{O:P}$. Dissolved oxygen exchanges with the atmosphere in the surface layer (F_{sfc}) according to the OCMIP protocol.

[47] Oxygen consumption in suboxic waters (<5 μM) is inhibited, according to

$$r_{sox}^{O2} = 0.5[\tanh(\mathrm{O}_2 - 5) + 1] \quad \text{(A17)}$$

but is replaced by the oxygen-equivalent oxidation of nitrate,

$$r_{sox}^{NO3} = 0.5[1 - \tanh(\mathrm{O}_2 - 5)]. \quad \text{(A18)}$$

Denitrification consumes nitrate at a rate of 80% of the oxygen equivalent rate, as NO_3 is a more efficient oxidant on a mol per mol basis (i.e., 1 mol of NO_3 can accept 5e$^-$ while 1 mol of O_2 can accept only 4 e$^-$). Note that the model does not include sedimentary denitrification, which would provide a large and less time-variant sink for fixed nitrogen. Because sedimentary denitrification would not change the qualitative dynamics of the model's behavior, but would slow the integration time, it is not included in the version presented here.

[48] **Acknowledgments.** Thanks to T. Westberry, T. Lenton, K. Kohfeld. and C. Le Quere for helpful comments. AS is supported by the Paleoclimate program of the National Science Foundation (ATM-0602395).

References

Annan, J. D., and J. C. Hargreaves (2006), Using multiple observationally-based constraints to estimate climate sensitivity, *Geophys. Res. Lett.*, *33*, L06704, doi:10.1029/2005GL025259.

Archer, D., and A. Ganopolski (2005), A movable trigger: Fossil fuel CO_2 and the onset of the next glaciation, *Geochem. Geophys. Geosyst.*, *6*, Q05003, doi:10.1029/2004GC000891.

Archer, D., H. Kheshi, and E. Maier-Reimer (1998), Dynamics of fossil fuel CO_2 neutralization by marine $CaCO_3$, *Global Biogeochem. Cycles*, *12*, 259–276.

Berelson, W. M. (2002), Particle settling rates increase with depth in the ocean, *Deep Sea Res., Part II*, *49*, 237–251.

Bitz, C. M., M. M. Holland, A. J. Weaver, and M. Eby (2001), Simulating the ice-thickness distribution in a coupled climate model, *J. Geophys. Res.*, *106*, 2441–2463.

Bolin, B., et al. (2000), Global perspective, in *Land Use, Land-Use Change, and Forestry: A Special Report of the Intergovernmental Panel on Climate Change*, edited by R. T. Watson et al., pp. 23–51, Cambridge Univ. Press, New York.

Bopp, L., P. Monfray, O. Aumont, J.-L. Dufresne, H. Le Treut, G. Madec, L. Terray, and J. C. Orr, (2001), Potential impact of climate change on marine export production, *Global Biogeochem. Cycles*, *15*, 81–100.

Cavalieri, D. J., P. Gloersen, C. L. Parkinson, J. C. Comiso, and H. J. Zwally (1997), Observed asymmetry in global sea ice changes, *Science*, *278*, 1104–1106.

Clark, P. U., S. W. Hostetler, N. G. Pisias, A. Schmittner, and K. J. Meissner (2007), Mechanisms for a ~7-kyr climate and sea-level oscillation during Marine Isotope Stage 3, in *Ocean Circulation: Mechanisms and Impacts*, *Geophys. Monogr. Ser.*, vol. 173, edited by A. Schmittner, J. Chiang, and S. Hemming, pp. 207–246, AGU, Washington, D. C.

Cox, P. M., R. A. Betts, C. D. Jones, S. A. Spall, and I. J. Totterdell (2000), Acceleration of global warming due to carbon-cycle feedbacks in a coupled climate model, *Nature*, *408*, 184–187.

Crowley, T. J. (2000), Causes of climate change over the past 1000 years, *Science*, *289*, 270–277.

Dufresne, J.-L., L. Fairhead, H. Le Treut, M. Berthelot, L. Bopp, P. Ciais, P. Friedlingstein, and P. Monfray (2002), On the magnitude of positive feedback between future climate change and the carbon cycle, *Geophys. Res. Lett.*, *29*(10), 1405, doi:10.1029/2001GL013777.

Eppley, R. W. (1972), Temperature and phytoplankton growth in the sea, *Fish. Bull.*, *70*, 1063–1085.

Ewen, T. L., A. J. Weaver, and M. Eby (2004), Sensitivity of the inorganic ocean carbon cycle to future climate warming in the UVic coupled model, *Atmos. Ocean*, *42*, 23–42.

Flueckiger, J., T. Blunier, B. Stauffer, J. Chappellaz, R. Spahni, K. Kawamura, J. Schwander, T. F. Stocker, and D. Dahl-Jensen (2004), N_2O and CH_4 variations during the last glacial epoch: Insight into global processes, *Global Biogeochem. Cycles*, *18*, GB1020, doi:10.1029/2003GB002122.

Frankignoulle, M., C. Canon, and J.-P. Gattuso (1994), Marine calcification as a source of carbon dioxide: Positive feedback of increasing atmospheric CO_2, *Limnol. Oceanogr.*, *39*, 458–462.

Friedlingstein, P., J.-L. Dufresne, P. M. Cox, and P. Rayner (2003), How positive is the feedback between climate change and the carbon cycle?, *Tellus, Ser. B*, *55*, 692–700.

Friedlingstein, P., et al. (2006), Climate-carbon cycle feedback analysis: Results from the C4MIP model intercomparison, *J. Clim.*, *19*, 3337–3353.

Fyfe, J. C., and O. A. Saenko (2005), Human-induced change in the Antarctic Circumpolar Current, *J. Clim.*, *18*, 3068–3073.

Gehlen, M., R. Gangsto, B. Schneider, L. Bopp, O. Aumont, and C. Ethe (2007), The fate of pelagic $CaCO_3$ production in a high CO_2 ocean: A model study, *Biogeosci. Disc.*, *4*, 534–560.

Gent, P. R., and J. C. McWilliams (1990), Isopycnal mixing in ocean circulation models, *J. Phys. Oceanogr.*, *20*, 150–155.

Govindasamy, B., S. Thompson, A. Mirin, M. Wickett, K. Caldeira, C. Delire, and P. B. Duffy (2005), Increase of carbon cycle feedback with climate sensitivity: Results from a coupled climate and carbon cycle model, *Tellus, Ser. B*, *57*, 153–163.

Grantham, B. A., F. Chan, K. J. Nielsen, D. S. Fox, J. A. Barth, A. Huyer, J. Lubchenco, and B. A. Menge (2004), Nearshore upwelling-driven hypoxia signals ecosystem and oceanographic changes in the NE Pacific, *Nature*, *429*, 749–754.

Heinze, C. (2004), Simulating oceanic $CaCO_3$ export production in the greenhouse, *Geophys. Res. Lett.*, *31*, L16308, doi:10.1029/2004GL020613.

Hirsch, A. I., A. M. Michalak, L. M. Bruhwiler, W. Peters, E. J. Dlugokencky, and P. P. Tans (2006), Inverse modeling estimates of the global nitrous oxide surface flux from 1998–2001, *Global Biogeochem. Cycles*, *20*, GB1008, doi:10.1029/2004GB002443.

Houghton, R. (2003), Revised estimates of the annual net flux of carbon to the atmosphere from changes in land use and land management 1850–2000, *Tellus, Ser. B*, *55*, 378–390.

IPCC (1995), *Climate Change 1995: The Science of Climate Change. Contribution of Working Group I to the Second Assessment Report of the Intergovernmental Panel on Climate Change*, edited by J. T. Houghton et al., 572 pp., Cambridge Univ. Press, New York.

IPCC (2001), *Climate Change 2001: The Scientific Basis. Contribution of Working Group I to the Third Assessment Report of the Intergovernmen-*

tal Panel on Climate Change, edited by J. T. Houghton et al., 881 pp., Cambridge Univ. Press, New York.

IPCC (2007), *Climate Change 2007: The Physical Science Basis. Contribution of Working Group I to the Fourth Assessment Report of the Intergovernmental Panel on Climate Change*, edited by S. Solomon et al., 996 pp., Cambridge Univ. Press, New York.

Jin, X., N. Gruber, J. P. Dunne, J. L. Sarmiento, and R. A. Armstrong (2006), Diagnosing the contribution of phytoplankton functional groups to the production and export of particulate organic carbon, $CaCO_3$, and opal from global nutrient and alkalinity distributions, *Global Biogeochem. Cycles*, *20*, GB2015, doi:10.1029/2005GB002532.

Jones, C. D., P. M. Cox, R. L. H. Essery, D. L. Roberts, and M. J. Woodage (2003), Strong carbon cycle feedbacks in a climate model with interactive CO_2 and sulphate aerosols, *Geophys. Res. Lett.*, *30*(9), 1479, doi:10.1029/2003GL016867.

Jones, P. D., T. J. Osborn, K. R. Briffa, C. K. Folland, B. Horton, L. V. Alexander, D. E. Parker, and N. Rayner (2001), Accounting for sampling density in grid-box land and ocean surface temperature time series, *J. Geophys. Res.*, *106*, 3371–3380.

Joos, F., G.-K. Plattner, T. F. Stocker, O. Marchal, and A. Schmittner (1999), Global warming and marine carbon cycle feedbacks on future atmospheric CO_2, *Science*, *284*, 464–467.

Joos, F., I. C. Prentice, S. Sitch, R. Meyer, G. Hooss, G.-K. Plattner, S. Gerber, and K. Hasselmann (2001), Global warming feedbacks on terrestrial carbon uptake under the Intergovernmental Panel on Climate Change (IPCC) emission scenarios, *Global Biogeochem. Cycles*, *15*, 891–908.

Jungclaus, J. H., H. Haak, M. Esch, E. Roeckner, and J. Marotzke (2006), Will Greenland melting halt the thermohaline circulation?, *Geophys. Res. Lett.*, *33*, L17708, doi:10.1029/2006GL026815.

Key, R. M., A. Kozyr, C. L. Sabine, K. Lee, R. Wanninkhof, J. L. Bullister, R. A. Feely, F. J. Millero, C. Mordy, and T.-H. Peng (2004), A global ocean carbon climatology: Results from Global Data Analysis Project (GLODAP), *Global Biogeochem. Cycles*, *18*, GB4031, doi:10.1029/2004GB002247.

Knutti, R., T. F. Stocker, F. Joos, and G.-K. Plattner (2003), Probabilistic climate change projections using neural networks, *Clim. Dyn.*, *21*, 257–272.

Langer, G., M. Geisen, K.-H. Baumann, J. Kläs, U. Riebesell, S. Thoms, and J. R. Young (2006), Species-specific responses of calcifying algae to changing seawater carbonate chemistry, *Geochem. Geophys. Geosyst.*, *7*, Q09006, doi:10.1029/2005GC001227.

Large, W. G., G. Danabasoglu, J. C. McWilliams, P. R. Gent, and F. O. Bryan (2001), Equatorial circulation of a global ocean climate model with anisotropic horizontal viscosity, *J. Phys. Oceanogr.*, *31*, 518–536.

Law, C. S., and N. J. P. Owens (1990), Significant flux of atmospheric nitrous oxide from the northwest Indian Ocean, *Nature*, *348*, 826–828.

Lee, K. (2001), Global net community production estimated from the annual cycle of surface water total dissolved inorganic carbon, *Limnol. Oceanogr.*, *46*, 1287–1297.

Lenton, T. M., et al. (2006), Millennial timescale carbon cycle and climate change in an efficient Earth system model, *Clim. Dyn.*, *26*, 687–711.

Levitus, S., J. Antonov, and T. Boyer (2005), Warming of the world ocean, 1955–2003, *Geophys. Res. Lett.*, *32*, L02604, doi:10.1029/2004GL021592.

Loutre, M. F., and A. Berger (2000), Future climatic changes: Are we entering an exceptional long interglacial?, *Clim. Change*, *46*, 61–90.

Maier-Reimer, E., U. Mikolajewicz, and A. Winguth (1996), Future ocean uptake of CO_2: Interaction between ocean circulation and biology, *Clim. Dyn.*, *12*, 711–722.

Marland, G., T. A. Boden, and R. J. Andres (2006), *In Trends: A Compendium of Data on Global Change, Carbon Dioxide Information Analysis Center*, Oak Ridge Natl. Lab., U. S. Dep. of Energy, Oak Ridge, Tenn.

Matear, R. J., and A. C. Hirst (1999), Climate change feedback on the future oceanic CO_2 uptake, *Tellus, Ser. B*, *51*, 722–733.

Matear, R. J., and A. C. Hirst (2002), Long-term changes in dissolved oxygen concentrations in the ocean caused by protracted global warming, *Global Biogeochem. Cycles*, *17*(4), 1125, doi:10.1029/2002GB001997.

Matsumoto, K., et al. (2004), Evaluation of ocean carbon cycle models with data-based metrics, *Geophys. Res. Lett.*, *31*, L07303, doi:10.1029/2003GL018970.

Matthews, H. D., A. J. Weaver, K. J. Meissner, N. P. Gillett, and M. Eby (2005a), Natural and anthropogenic climate change: Incorporating historical land cover change, vegetation dynamics and the global carbon cycle, *Clim. Dyn.*, *22*, 461–479.

Matthews, H. D., A. J. Weaver, and K. J. Meissner (2005b), Terrestrial carbon cycle dynamics under recent and future climate change, *J. Clim.*, *18*, 1609–1628.

Matthews, H. D., M. Eby, T. Ewen, P. Friedlingstein, and B. J. Hawkins (2007), What determines the magnitude of carbon cycle-climate feedbacks?, *Global Biogeochem. Cycles*, *21*, GB2012, doi:10.1029/2006GB002733.

Meissner, K. J., A. J. Weaver, H. D. Matthews, and P. M. Cox (2003), The role of land surface dynamics in glacial inception: A study with the UVic Earth System Model, *Clim. Dyn.*, *21*, 515–537.

Moisan, J. R., T. A. Moisan, and M. R. Abbott (2002), Modelling the effect of temperature on the maximum growth rates of phytoplankton populations, *Ecol. Modell.*, *153*, 197–215.

Montoya, J. P., E. J. Carpenter, and D. G. Capone (2002), Nitrogen fixation and nitrogen isotope abundances in zooplankton of the oligotrophic North Atlantic, *Limnol. Oceanogr.*, *47*, 1617–1628.

Moore, J. K., S. C. Doney, J. A. Kleypas, D. M. Glover, and I. Y. Fung (2002), An intermediate complexity marine ecosystem model, *Deep Sea Res., Part II*, *49*, 403–462.

Nakicenovic, N., et al. (2000), *IPCC Special Report on Emissions Scenarios*, edited by N. Nakicenovic and R. Swart, 570 pp., Cambridge Univ. Press, New York.

Nevison, C., J. H. Butler, and J. W. Elkins (2003), Global distribution of N_2O and the delta N_2O-AOU yield in the subsurface ocean, *Global Biogeochem. Cycles*, *17*(4), 1119, doi:10.1029/2003GB002068.

Orr, J. C., R. Najjar, C. L. Sabine, and F. Joos (1999), Abiotic-HOWTO, internal OCMIP report, LSCE/CEA Saclay, 25 pp., Gif-sur-Yvette, France.

Orr, J. C., et al. (2005), Anthropogenic ocean acidification over the twenty-first century and its impact on calcifying organisms, *Nature*, *437*, 681–686.

Plattner, G.-K., F. Joos, and T. F. Stocker (2002), Revision of the global carbon budget due to changing air-sea oxygen fluxes, *Global Biogeochem. Cycles*, *16*(4), 1096, doi:10.1029/2001GB001746.

Prather, M., et al. (2001), Atmospheric chemistry and greenhouse gases, in *Climate Change 2001: The Scientific Basis. Contribution of Working Group I to the Third Assessment Report of the Intergovernmental Panel on Climate Change*, edited by J. R. Houghton et al., 881 pp., Cambridge Univ. Press, New York.

Ramankutty, N., and J. A. Foley (1999), Estimating historical changes in land cover: Croplands from 1700 to 1992, *Global Biogeochem. Cycles*, *13*, 997–1027.

Ramaswamy, V., O. Boucher, J. Haigh, D. Hauglustaine, J. Haywood, G. Myhre, T. Nakajima, G. Y. Shi, and S. Solomon (2001), Radiative forcing of climate change, in *Climate Change 2001: The Scientific Basis. Contribution of Working Group I to the Third Assessment Report of the Intergovernmental Panel on Climate Change*, edited by J. R. Houghton et al., 881 pp., Cambridge Univ. Press, New York.

Ridgwell, A., and J. C. Hargreaves (2007), Regulation of atmospheric CO_2 by deep-sea sediments in an Earth system model, *Global Biogeochem. Cycles*, *21*, GB2008, doi:10.1029/2006GB002764.

Ridgwell, A., I. Zondervan, J. C. Hargreaves, J. Bijma, and T. M. Lenton (2006), Significant long-term increase of fossil fuel CO_2 uptake from reduced marine calcification, *Biogeosci. Disc.*, *3*, 1763–1780.

Riebesell, U., I. Zondervan, B. Rost, P. D. Tortell, R. E. Zeebe, and F. M. Morel (2000), Reduced calcification of marine plankton in response to increased atmospheric CO_2, *Nature*, *407*, 311–313.

Russell, J. L., K. W. Dixon, A. Gnanadesikan, R. J. Stouffer, and J. R. Toggweiler (2006), The Southern Hemisphere westerlies in a warming world: Propping open the door to the deep ocean, *J. Clim.*, *19*, 6382–6390.

Sabine, C. L., et al. (2004), The oceanic sink for anthropogenic CO_2, *Science*, *305*, 367–371.

Saenko, O. A., A. Schmittner, and A. J. Weaver (2002), On the role of wind driven sea ice motion on ocean ventilation, *J. Phys. Oceanogr.*, *32*, 3376–3395.

Sanudo-Wilhelmy, S. A., A. Tovar-Sanchez, F.-X. Fu, D. G. Capone, E. J. Carpenter, and D. A. Hutchins (2004), The impact of surface-adsorbed phosphorus on phytoplankton Redfield stoichiometry, *Nature*, *432*, 897–901.

Sarmiento, J. L., T. M. C. Hughes, R. J. Stouffer, and S. Manabe (1998), Simulated response of the ocean carbon cycle to anthropogenic climate warming, *Nature*, *393*, 245–249.

Sarmiento, J. L., J. Dunne, A. Gnanadesikan, R. M. Key, K. Matsumoto, and R. Slater (2002), A new estimate of the $CaCO_3$ to organic carbon export ratio, *Global Biogeochem. Cycles*, *16*(4), 1107, doi:10.1029/2002GB001919.

Sarmiento, J. L., et al. (2004), Response of ocean ecosystems to climate warming, *Global Biogeochem. Cycles*, *18*, GB3003, doi:10.1029/2003GB002134.

Schartau, M., and A. Oschlies (2003), Simultaneous data-based optimization of a 1D-ecosystem model at three locations in the North Atlantic. part I: Method and parameter estimates, *J. Mar. Res.*, *61*, 765–793.

Schmittner, A. (2005), Decline of the marine ecosystem caused by a reduction in the Atlantic overturning circulation, *Nature*, *443*, 628–633.

Schmittner, A., K. J. Meissner, M. Eby, and A. J. Weaver (2002a), Forcing of the deep ocean circulation in simulations of the Last Glacial Maximum, *Paleoceanography*, *17*(2), 1015, doi:10.1029/2001PA000633.

Schmittner, A., M. Yoshimori, and A. J. Weaver (2002b), Instability of glacial climate in a model of the ocean-atmosphere-cryosphere system, *Science*, *295*, 1489–1493.

Schmittner, A., O. A. Saenko, and A. J. Weaver (2003), Coupling of the hemispheres in observations and simulations of glacial climate change, *Quat. Sci. Rev.*, *22*, 659–671.

Schmittner, A., A. Oschlies, X. Giraud, M. Eby, and H. L. Simmons (2005a), A global model of the marine ecosystem for long term simulations: Sensitivity to ocean mixing, buoyancy forcing, particle sinking and dissolved organic matter cycling, *Global Biogeochem. Cycles*, *19*, GB3004, doi:10.1029/2004GB002283.

Schmittner, A., M. Latif, and B. Schneider (2005b), Model projections of the North Atlantic thermohaline circulation for the 21st century assessed by observations, *Geophys. Res. Lett.*, *32*, L23710, doi:10.1029/2005GL024368.

Schmittner, A., E. D. Galbraith, S. Hostetler, T. F. Pedersen, and R. Zhang (2007a), Large fluctuations of dissolved oxygen in the Indian and Pacific oceans during Dansgaard-Oeschger oscillations caused by variations of North Atlantic Deep Water subduction, *Paleoceanography*, *22*, PA3207, doi:10.1029/2006PA001384.

Schmittner, A., E. J. Brook, and J. Ahn (2007b), Impact of the ocean's overturning circulation on atmospheric CO_2, in *Ocean Circulation: Mechanisms and Impacts*, *Geophys. Monogr. Ser.*, vol. 173, edited by A. Schmittner, J. Chiang, and S. Hemming, pp. 315–334, AGU, Washington, D. C.

Simmons, H. L., S. R. Jayne, L. C. St. Laurent, and A. J. Weaver (2004), Tidally driven mixing in a numerical model of the ocean general circulation, *Ocean Modell.*, *6*, 245–263.

Swingedouw, D., P. Braconnot, and O. Marti (2006), Sensitivity of the Atlantic Meridional Overturning Circulation to the melting from northern glaciers in climate change experiments, *Geophys. Res. Lett.*, *33*, L07711, doi:10.1029/2006GL025765.

Takahashi, T., et al. (2002), Global sea-air CO_2 flux based on climatological surface ocean pCO_2, and seasonal biological and temperature effects, *Deep Sea Res., Part II*, *49*, 1601–1622.

Taylor, K. E. (2001), Summarizing multiple aspects of model performance in a single diagram, *Geophys. Res. Lett.*, *106*, 7183–7192.

Tyrell, T. (1999), The relative influence of nitrogen and phosphorus on oceanic primary production, *Nature*, *400*, 525–531.

Weaver, A. J., M. Eby, A. F. Fanning, and E. C. Wiebe (1998), Simulated influence of carbon dioxide, orbital forcing and ice sheets on the climate of the Last Glacial Maximum, *Nature*, *394*, 847–853.

Weaver, A. J., et al. (2001), The UVic Earth system climate model: Model description, climatology and applications to past, present and future climates, *Atmos. Ocean*, *4*, 361–428.

Wigley, T. M. L. (2005), The climate change commitment, *Science*, *307*, 1766–1769.

Yamagishi, H., N. Yoshida, S. Toyoda, B. N. Popp, M. B. Westley, and S. Watanabe (2005), Contributions of denitrification and mixing on the distribution of nitrous oxide in the North Pacific, *Geophys. Res. Lett.*, *32*, L04603, doi:10.1029/2004GL021458.

Zeng, N., H. Qian, E. Munoz, and R. Iacono (2004), How strong is carbon cycle-climate feedback under global warming?, *Geophys. Res. Lett.*, *31*, L20203, doi:10.1029/2004GL020904.

E. D. Galbraith, Atmospheric and Oceanic Sciences, Princeton University, 300 Forrestal Road, Princeton, NJ 08540, USA.

H. D. Matthews, Planning and Environment, Concordia University, 1455 de Maisonneuve Boulevard West, Montreal, Quebec, H3G 1M8, Canada.

A. Oschlies, Leibniz Institute of Marine Sciences at the Christian-Albrechts University of Kiel (IFM-GEOMAR), Düsternbrooker Weg 20, 24105 Kiel, Germany.

A. Schmittner, College of Oceanic and Atmospheric Sciences, Oregon State University, 104 COAS Admin Building, Corvallis, OR 97331-5503, USA.